EUROPEAN RESPIRATORY *journal*

FLAGSHIP SCIENTIFIC JOURNAL OF ERS

Early View

Original article

An integrated multiomic and quantitative label-free microscopy-based approach to study pro-fibrotic signalling in *ex vivo* human precision-cut lung slices

Muzamil Majid Khan, Daniel Poeckel, Aliaksandr Halavatyi, Joanna Zukowska-Kasprzyk, Frank Stein, Johanna Vappiani, Daniel C. Sevin, Christian Tischer, Nico Zinn, Jessica D Eley, Natasja Stæhr Gudmann, Thomas Muley, Hauke Winter, Andrew J Fisher, Carmel B. Nanthakumar, Giovanna Bergamini, Rainer Pepperkok

Please cite this article as: Khan MM, Poeckel D, Halavatyi A, *et al*. An integrated multiomic and quantitative label-free microscopy-based approach to study pro-fibrotic signalling in *ex vivo* human precision-cut lung slices. *Eur Respir J* 2020; in press (https://doi.org/10.1183/13993003.00221-2020).

An integrated multiomic and quantitative label-free microscopy-based approach to study pro-fibrotic signalling in *ex vivo* human precision-cut lung slices

Muzamil Majid Khan[1,2,5], Daniel Poeckel[2], Aliaksandr Halavatyi[1,5], Joanna Zukowska-Kasprzyk[1], Frank Stein[1], Johanna Vappiani[2], Daniel C. Sevin[2], Christian Tischer[1], Nico Zinn[2], Jessica D Eley[4], Natasja Stæhr Gudmann[3], Thomas Muley[5,6], Hauke Winter[5,6], Andrew J Fisher[7], Carmel B. Nanthakumar[4], Giovanna Bergamini[2]*, Rainer Pepperkok[1,5]*

[1] European Molecular Biology Laboratory, Meyerhofstrasse 1, Heidelberg, Germany, [2] Discovery Biology, Cellzome GmbH, GSK, Heidelberg, Germany, [3] Nordic Bioscience, Herlev, Denmark, [4] Novel human genetics research unit, GSK, Stevenage, UK, [5] Lung Research Center Heidelberg (TLRC), German Center for Lung Research (DZL), Heidelberg, Germany, [6] Biobank Thoraxklinik, University Hospital Heidelberg, Heidelberg, Germany [7] Newcastle University Translational and Clinical Research Institute and Institute of Transplantation, Newcastle Upon Tyne Hospitals, Newcastle upon Tyne, UK

*corresponding authors

Abstract:
Fibrosis can affect any organ resulting in the loss of tissue architecture and function with often life-threatening consequences. Pathologically, fibrosis is characterised by expansion of connective tissue due to excessive deposition of extracellular matrix proteins (ECM), including the fibrillar forms of collagen. A significant limitation for discovering cures for fibrosis is the availability of suitable human models and techniques to quantify mature fibrillar collagen deposition as close as possible to human physiological conditions. Here we have extensively characterised an *ex vivo* cultured human lung tissue-derived, precision-cut lung slices model (hPCLS) using label-free second harmonic (SHG) light microscopy to quantify fibrillar collagen deposition and mass spectrometry-based techniques to obtain a proteomic and metabolomic fingerprint of hPCLS in *ex vivo* culture.
We demonstrate that hPCLS are viable and metabolically active with mesenchymal, epithelial, endothelial, and immune cell types surviving for at least two weeks in *ex vivo* culture. Analysis of hPCLS-conditioned supernatants showed a strong induction of pulmonary fibrosis-related ECM proteins upon TGFß1 stimulation. This upregulation of ECM proteins was not translated into an increased deposition of fibrillar collagen. In support of this observation, we revealed the presence of a pro-ECM degradation activity in our *ex vivo* cultures of hPCLS, inhibition of which by metalloproteinase inhibitor resulted in increased collagen deposition in response to TGFß1 stimulation. Together the data show that an integrated approach of measuring soluble pro-fibrotic markers alongside quantitative SHG-based analysis of fibrillar collagen is a valuable tool for studying pro-fibrotic signalling and testing antifibrotic agents.

Introduction:
Excessive deposition of extracellular matrix proteins is a hallmark of fibrosis. This leads to alteration of tissue architecture, subsequently loss of its function and ultimately to end-stage organ failure[1]. In the developed world, 45% of all deaths are attributed to conditions related to an excess of ECM deposition[2]. While fibrosis contributes to exacerbated pathology in cancer, myocardial infarctions and ageing, it is also a primary cause of mortality in the fibrotic disease of kidneys, liver and lung in particular[3]. Chronic interstitial lung diseases (ILDs) are the most common form of

pulmonary fibrosis (*European Respiratory Society*). ILDs have been subdivided into over 300 subtypes, among which idiopathic pulmonary fibrosis (IPF) is the most prevalent (*European Respiratory Society*). Upon damage of epithelial and endothelial cells in various organs, an inflammatory response is launched, which triggers blood clot formation and ECM repair. Part of this repair mechanism is the release of cytokines such as TGFß1 that initiate the activation of macrophages and fibroblasts[3]. Activated fibroblasts express alpha-SMA, which leads to their differentiation in myofibroblasts[3]. Persistent chronic inflammation triggers unchecked proliferation of myofibroblasts, increased epithelial to mesenchymal cell type transition [3]. The mesenchymal population of cells have an enhanced ability to produce ECM components, and a combination of these events result in a derailed tissue repair process leading to tissue scarring[3]. TGFß1 is considered to be the master regulator of the signalling pathways (pro-fibrotic) that lead to an abnormally excessive deposition of extracellular matrix[4]. Induction of pro-fibrotic signalling also shifts the delicate balance between synthesis and breakdown of collagens and other ECM[5] proteins in favour of excessive deposition and pathological stiffening of ECM with loss of tissue compliance. This excessive deposition and stiffness of ECM causes a physical abnormality that leads to atrophying of alveolar tissue[3] and subsequent suffocation (dyspnea). In IPF patients, the fibrotic foci are characterised by an abnormally high content of fibrillar collagen (type I, III and V)[3,6]. At the ECM level, presence of these fibrillar collagens are the physical cause of eventual mortality[7]. Despite our understanding of the molecular basis underlying the fibrotic process, to date only two licensed drugs; pirfenidone and nintedanib[8] are approved for the treatment of IPF. These medicines have very low efficacy and hence high patient withdrawal rates[9]. The lack of more effective antifibrotic therapies may be attributed in part (a) to the absence of adequate model systems that can mimic the pathophysiology of the fibrotic process as related to human physiology[10], (b) to indirect functional readouts of biomarkers used for quantifying disease progression. Currently, murine experimental models of fibrosis are frequently used to study lung, liver and kidney fibrosis. Typically, pulmonary fibrosis is induced either using genetic manipulation such as MUC5b overexpression, a genetic risk factor identified in large cohorts of IPF patients[11] or chemical induction (bleomycin sulphate, amiodarone, carbon tetrachloride[12]. While these model systems help to understand acute signalling pathways preceding tissue damage and, in some instances, chemicals such as bleomycin sulphate can be used as causative agents[13] but, *in vivo* models lack histological features of human disease and can spontaneously resolve, therefore failing to recapitulate the irreversible end-stage disease. These model systems have highlighted an inflammatory component present during the development of fibrotic disease, yet anti-inflammatory drugs have failed in clinical development[14,15]. Based on these findings, therapies involving corticosteroids (prednisone) with or without immunosuppressive drugs (azathioprine and cyclophosphamide) were used to treat IPF. In fact, some drugs have had adverse effects that worsen patient condition[14,15].

Human precision-cut lung slices (hPCLS) are 3-dimensional, uniformly cut slices of lung tissue that may be maintained in *ex vivo* culture that have emerged as a promising potential model system to study human disease *in vitro*. PCLS (rat lung and human) came into existence in the early 1990s[16,17] but have only recently been used as a model for evaluating human disease pathophysiology[10,18]. Several groups have used this model system to recapitulate pro-fibrotic signalling[10,18,19] , and recently Akram et al[20] have studied the dynamics of epithelial cells in mouse PCLS. However, the overall molecular changes, molecular pathways changing in *ex vivo*

culture of human PCLS are still elusive. Earlier studies[10,18] do show an induction in fibrotic signalling, but a functional readout of enhanced ECM deposition has been lacking. Furthermore, whether cell types essential for fibrosis such as epithelial, mesenchymal and immune cell types[3] are present in the model system has not been investigated. Although, it is generally assumed that in hPCLS cell/cell and cell/matrix interactions are well preserved[20], no systematic study has been conducted to evaluate such a hypothesis.

ELISA based measurements of cleavage products of collagen propeptides such as type I or III and VI, collagen can be quantified as they are cleaved off during formation. These cleavage products reveal information on fibrosis disease progression[21]. While these markers could prove to be disease biomarkers, their correlation/ dynamics to excess deposition is still not established. Microscopic detection of fibrillar collagen is also difficult due to lack of specific antibodies. However, label-free second harmonic generation imaging for fibrillar collagen has been shown to be an excellent alternative method for quantifying fibrillar collagen in tissue slices[22].

Therefore, in this study using mass spectrometry and light microscopy-based approaches we first sought to investigate and characterise the changes of protein expression in the four major cell types present in lung tissue when hPCLS are *ex vivo* cultured. Second, to investigate the pro-fibrotic signalling induced by TGFß1 stimulation, we established a new, quantitative, label-free second harmonic generation imaging approach that quantifies deposited fibrillar collagen in the extracellular matrix upon pro-fibrotic stimulation. We propose that this model represents a versatile human translational model system that could be used for identifying and characterizing antifibrotic agents.

Results:

Proteomic characterisation of molecular changes in hPCLS over time in *ex vivo* culture conditions.

To use hPCLSs, derived from tissue resection of non-ILD patients, for mimicking a particular disease involving certain cell types and signalling pathways, it is imperative to characterise this model system in given *ex vivo* culture conditions. To this end, we used mass spectrometry-based proteomics and untargeted metabolomics to monitor the hPCLS proteome and metabolome over time in *ex vivo* culture. *Ex vivo* cultured hPCLS (4 donors, 2 replicates/ donor, 2 hPCLS/ replicate) were harvested on different days (day 1, 4, 7, 10 and 13 in culture) and snap-frozen in liquid nitrogen. Subsequently, lysates were prepared for mass spectrometry-based proteomic and metabolomic analysis. For proteomic analysis, 2 % SDS soluble fractions of hPCLS were subjected to LC/MS analysis. Approximately 5500 proteins were detected across the 4 donors tested, and of those, 4288 proteins were in common (Table S1). These proteins could be attributed to different cellular localisation bioinformatically using GeneOntology database[23]. The percentage of proteins per GO term is calculated relative to the whole GO term independent of its expression in human lung tissue. Here, 3648 (31.75%, reference list of 11488 proteins- GO: 0005737) were cytoplasmic, 2556 (25.9 %, reference list of 9856 proteins- GO: 0016020) were membrane, 1149 (54.2 %, reference list of 2119 proteins- GO: 1903561) were extracellular vesicle related and 207 (38.6%, reference list of 536 proteins-GO: 0031012) were extracellular matrix related. 187 proteins (45.7 %, reference list of 409 proteins- GO: 0062023) could be associated with the collagen-containing extracellular matrix GO term. It should be noted that the number of proteins (3648,

2556, 1149 and 207) do not add up to 5500, as many of the proteins are classified as belonging to more than one GO term.

Differential analysis (Figure 2A) of log2 fold changes in protein levels with respect to the previous time point of harvest shows that hPCLS undergo significant changes. In total, on day 13, 728 (17%, TableS1) out of the 4288 proteins change significantly compared to day 1. Of these, 10% change from day 1 to day 4 and the remaining 7% from day 4 to day 7. Between day 7 and 13 no further changes were observed. In total, 343 out of the 728 changing proteins were downregulated and 385 were upregulated.

Cytoscape based network analysis (FigureS2B) of the 728 proteins showed primarily an upregulation of pathways involving proteins related to ECM degradation. Fewer pathways are related to the formation of ECM. A significant upregulation of inflammatory signalling pathways, such as neutrophil degranulation and innate immune system were also observed (FigureS2B).

We further analysed the proteomics data to investigate the dynamics of different cell types underlying the observed changes in protein levels. Human lung tissue is mainly composed of immune, mesenchymal, endothelial and epithelial cells. **L**ung **G**ene **E**xpression **A**nalysis (LGEA) web portal has established a database of gene expression of each cell type (also age-dependent, from neonatal to adult stages) in both mouse and human lungs[24,25]. In this database, the RNA-seq of flow-sorted human lung cells have been designated as CD45+ immune cells, CD45-/PECAM-/VECadherin-/EpCAM+ mixed epithelial cells, CD45-/PECAM+/VECadherin+ mixed endothelial cells and CD45-/PECAM-/VECadherin-/EpCAM- mixed mesenchymal cells. The parent list can be downloaded from LGEA data base under "LungSortedCells". We compared (Table S3) significantly changing (log2FC ≥0.5 and ≤-0.5 and fdr p-value ≤ 0.05) proteins on day 13 vs day 1 to the list of proteins attributed to different cell classes (in LGEA[25] analysis). Figure S2C shows markers for 4 broadly categorised major cell types, namely, Epithelial, Endothelial, Mesenchymal and Immune cell types which are typically present in lung tissues on day 13 in our culture system. Based on LGEA database we also curated a list of commonly used lung-cell type markers (Figure S2C, Table S3). Of note, AGER (alveolar type-I) and SFTPC (alveolar type -II) both are significantly downregulated in our *ex vivo* culture, while SFTPB, another alveolar type-II marker, shows significant up-regulation on day 13 compared to day 1. The majority of the detectable myofibroblasts markers show a persistent decrease while fibroblasts markers TNC, PDGFRA, show an increase and VIM shows no change. ACTA2 a further well-established marker of myofibroblasts could not be detected.

Among the significantly changing mesenchymal proteins, pro-fibrotic collagens[7] such COL5A1 (Log2FC -0.7) and COL3A1 (Log2FC -0.9) were significantly downregulated. Given that the collagen class of proteins is highly relevant for fibrosis progression[7], this observation prompted us to look into the pattern of regulation of all the collagens detected. The data shows that under the culture conditions used, the majority of the detected collagens (Figure 3) undergo downregulation over time including COL1, COL4 and COL6. Furthermore, there is a significant upregulation of MMP2 (Log2FC 2.1) and MMP14 (Log2FC 2.27), both are metalloproteinases involved in degrading fibrillar collagens[26] such as COLI, COLII, COLIII and COLV. TIMP2 and TIMP3, two tissue inhibitors of metalloproteinases[27] were also detected (Table S1). While TIMP3 did not show any major change (Log2FC -0.24 (fdr 0.507), day 13 vs day 1), TIMP2 was upregulated over time (Log2FC 2.39, fdr < 0.0001, day 13 vs day 1). In this context, it is important to note, that TIMP2 has been shown to enhance MMP2 activity[28,29], which is a degrading enzyme of collagens[30]**.**

In general, the metalloproteinases detected over the course of *ex vivo* culture show an upregulated expression (Figure 3).

Metabolomic analyses and live cell imaging demonstrate hPCLS viability over time in *ex vivo* culture.

To investigate whether hPCLS, derived from tissue resection of non-ILD patients, are metabolically active in *ex vivo culture* conditions, samples were harvested as for the proteomic analysis, and in addition, solubilised and mechanically homogenised to extract metabolites. *Ex- vivo* cultured hPCLS (3 donors, 2 replicates/ donor, 2 hPCLS/ replicate) were subjected to LC/MS-based untargeted metabolomic analysis [31]. A total of 3523 metabolites were detected reproducibly (Table S2) over the range of samples analysed. Out of these, 335 metabolites changed significantly in their abundance from day 1 to 13 (TableS2; Figure S2E).

Pathway analysis of the significantly changing annotated metabolites revealed no apparent enrichment of specific pathways. We analysed changes of selected metabolites sensitive to changes in tissue health. This showed that hPCLS are metabolically stable in *ex vivo* culture (Figure S2F). Specifically, adenosine triphosphate levels of the hPCLS remained unchanged, and L-Lactic acid levels significantly built up over time in culture, implicating a metabolically active 3D tissue system. Also, L-Glutamine was increasingly being metabolised by hPCLS without undergoing any oxidative stress, as depicted by stable levels of the redox-sensitive metabolites cysteine-glutathione disulfide and glutathione (Figure S2F).

To further assess tissue health in hPCLS *ex vivo* culture, we also performed live/ dead cell microscopy-based analysis. This showed that there is no change in the signal related to the number of living cells (Calcein AM) over time from day 1 to day 13 (Figure S2A), while the number of dead cells considerably decreased from day 1 to day 04 by 58% but remained constant from day 4 to day 13. The number of dead cells decreased from day 1 to day 7, and remained constant between day 7 and day 13, suggesting that there are always cells dying in the hPCLS culture. In contrast calcein AM signal did not change over time, suggesting active cell proliferation is taking place to replace dying cells (Figure S2A). This is further supported by constant adenosine triphosphate (ATP) metabolite levels over time (Figure S2F-G). Consistent with these data, proteomic analysis comparing day 13 vs day 1 (Figure S2B) show that pathways inhibiting cell proliferation are downregulated.

Induction of pro-fibrotic signalling upon TGFß1 stimulation in *ex vivo* hPCLS culture

TGFß1 is a cytokine regarded as a master regulator of fibrotic signalling[32]. To induce pro-fibrotic signalling in our culture system, we used TGFß1 (10ng/ml) as reported previously by other groups both in murine model systems[33] and hPCLS[10]. On day 1, 4, 7 and 10 (Figure 1), hPCLS, derived from tissue resection of non-ILD patients, were replenished with fresh medium containing human recombinant TGFß1 or vehicle in *ex vivo* culture. Supernatants from each hPCLS (±TGFß1) in culture were collected separately on day 4, day 7 and day 13. Per donor, 4 hPCLS conditioned supernatants (except for LT18, day 4) were separately subjected to proprietary competitive ELISA for detecting selected neoepitope[34] pro-fibrotic markers such as Procollagen 1 N- terminal propeptide (PRO-C1)[35], the C-terminal part of Fibronectin (FBN-C), Collagen type III degradation marker (C3M). Consistent with earlier studies[10,36], TGFß1 stimulation (Figure 4A) increased the level of PRO-C1 and FBN-C detected in the culture supernatants indicating induction of pro-fibrotic signalling, while C3M showed no changes.

To better characterise how the hPCLS model system would respond to TGFß1 stimulation, we also analysed the TGFß1 response at the proteomic level (4 donors, 2 replicates/ donor, 2 hPCLS/ replicate). Here, hPCLS (vehicle-treated and TGFß1 treated) were harvested on day 13 of *ex vivo* culture. The hPCLS were subjected to 2% SDS solubilisation and mechanical disruption. Subsequently, lysates were subjected to LC/MS. On average, a total of 6600 proteins per replicate and per donor were detected.

Amongst these, 3998 proteins were common across 8 replicates (4 donors; Table S4) and were subjected to further downstream analyses. Differential analysis of TGFß1 treated hPCLS compared to vehicle-treated hPCLS (day 13) was performed. The analysis that TGFß1 treatment resulted in a significant change of 109 proteins (Log2FC between 0.58 and -0.58, fdr p-value of 0.05 out of 3998, Figure S4A). A curated data analysis for proteins associated with fibrotic processes was done. This showed that proteins such as COL1A2, COL3A1, COL5A1, FBN-C, THBS1[37], THBS2[38] , VCAN and TNC[39], FKBP10[40] were significantly upregulated (Figure 4B). Furthermore, significantly changing proteins were subjected to pathway analysis using Cytoscape (Figure S4B). This showed induction of pro-fibrotic pathways such as embryonic morphogenesis, ECM organisation, interleukin signalling and downregulation of pro-epithelial injury signalling pathways such as surfactant metabolism[41–44]. Interestingly, proteomic analysis of peripheral blood done elsewhere from IPF patients has been shown to have downregulated cell proliferation[45]pathways, similar to the proteome of TGFß1 treated hPCLS analysed in our study.

The 109 proteins significantly regulated (Figure S4A) upon TGFß1 treatment were curated against LGEA database for cell-type specific markers (Table S5). This analysis shows that the majority of the significantly downregulated proteins (39 out of 44) are specific for epithelial cells while those upregulated (64 out of 65) are specific for mesenchymal cells suggesting that TGFß1 stimulation might induce an epithelial to mesenchymal-transition (EMT)-based pro-fibrotic signalling system[4] under the culture conditions used here. But to confirm it is indeed EMT, would need further analyses. Both, ELISA analyses for culture supernatant and the proteomic analyses of the cellular fraction, showed high upregulation of collagens upon TGFb1 stimulation (Figure 4A-B). In our proteomics data here, the typical myofibroblast marker alpha-smooth muscle actin (ACTA2) could not be detected, but other markers such as MYLK[25], TAGLN[25] did show significant upregulation (Table S4, Log2FC 0.52 and 0.6 9 respectively). These data are consistent with several recent studies[10,18,19] showing induction of pro-fibrotic signalling in *ex vivo* cultured hPCLS using TGFß1 stimulation[10] or a cocktail of pro-fibrotic factors[18].

Whether such up-regulation of pro-fibrotic factors with differential regulation of MMPs results in a consistent and specific ECM deposition (fibrillar collagen in particular) has so far not been tested. Therefore, we investigated next whether the observed upregulation of pro-fibrotic factors was translating into deposition of fibrillar collagens in the extracellular matrix.

Quantitative label-free Second Harmonic Generation (SHG) imaging analysis of fibrillar collagen

SHG microscopy is a label-free imaging method, in which individual non-centrosymmetric molecules generate a second harmonic signal when illuminated with short far-red laser pulses as they are used in 2-photon microscopy[46]. In human tissues, the acto-myosin complex of skeletal muscles (cytosolic)[47], large microtubules[48] (cytosolic) and fibrillar collagens[46] (extracellular matrix) have been

demonstrated to have the noncentrosymmetry required to generate SHG signals. Given the earlier findings that only large fibrillar collagen is present in the ECM of lung tissue[22], SHG imaging can be considered as a highly specific and a suitable technique for quantitative measurements of matrix deposition in hPCLS.
First, we compared hPCLS (PFA fixed on day 0), derived from tumour-free lung tissue of non-ILD patients, with those derived from end-stage interstitial lung disease [(Idiopathic pulmonary fibrosis (IPF) and Nonspecific interstitial pneumonia (NSIP)] patients. 250µm thick and 8mm in diameter hPCLS from day 0 were chemically fixed. The entire hPCLS were imaged (Figure 5A-C). Subsequently, the acquired 3D stacks were analysed using a semi-automated image analysis pipeline (Jython script-image analysis, available as supplementary material to this manuscript). The raw SHG intensity (SHGi) values (Figure S5A) of non-ILD and ILD patients are significantly different. However, to quantify these relative fold differences, integrated SHG signal (iSHG) was Log2 transformed (Log2iSHG) for each hPCLS, average of iSHG of all non-ILD hPCLS (4 non-ILD patients) was calculated and Log2 transformed (Log2iSHGc). Next, for each hPCLS the difference between Log2iSHG and Log2iSHGc was determined as Log2SHGi. The analysis showed significantly more deposited fibrillar collagen in ILD hPCLS compared to non-ILD controls. We observed the SHG signal originating from airways or blood vessels (Figure 5B*) was similar in intensity between non-ILD and ILD tissues, while the interstitial collagen signal (Figure 5B*) showed a dramatic increase in ILD compared to non-ILD conditions.

hPCLS have variable quantitative SHG signal due to spatial morphological differences.
Visual analysis of SHG images of whole hPCLS (PFA fixed, unstimulated, non-ILD patients, day 13) showed inherent heterogeneity of the SHG signal (Figure 5D). Clearly, different hPCLS have varied content of airways, blood vessels and lung interstitium. Therefore, based on our observation (Figure 5B) and previous reports that for fibrotic phenotypes in interstitial lung diseases, it is the parenchymal interstitium which is affected[49], we devised a two-way image analysis approach; (a) SHG intensity from whole hPCLS were analysed to compare differences and (b) we manually excluded from analysis, any region of interest (ROI) that had SHG signal originating from a blood vessel or an airway or didn't have any signal (purple Xs, Figure 5E). Hence, only the interstitium of the hPCLS was analysed to compare differences (Figure 5E). To quantitatively measure the differences in the two approaches, we used SHG images of unstimulated hPCLS, PFA fixed on day 13 of *ex vivo* culture. Using our image analysis pipeline, SHG intensity of whole hPCLS (whole) and just the interstitium (ROIs) were calculated (raw values whole hPCLS Figure S5B). To analyse fold differences, the raw values of SHG intensity (iSHG) of whole hPCLS or just the interstitial ROIs values were log2 transformed (Log2iSHG) normalised to the mean SHG intensity of unstimulated hPCLS (Log2iSHGc) of each donor. To analyse if the presence of heterogenous fibrillar collagen (originating from airways or blood vessels) makes the SHG signal more variable, we analysed the SHGintensity levels measured by whole hPCLS and ROI method (Figure 5F). Indeed, the variance of the whole (0.39) was 2 times higher compared to ROI analysis (0.19). Furthermore, only Log2SHGi values of fibrillar collagen from ROI analysis show normal distribution as per our normality tests (Table 2, Anderson-Darling, D'Agostino & Pearson test & Shapiro-Wilk test). The data shows that ROI analysis removes the inherent variability in hPCLS that comes from factors not relevant to the current analysis. These data suggest that if there are subtle change in

the interstitial fibrillar collagen taking place, ROI analysis will be better suited to quantify these changes.
We also analysed if there are gender, smoking status and age-related difference in interstitial collagen in unstimulated hPCLS after 13 days of ex vivo culture (Figure S5C). The analyses show that in male the average fibrillar collagen content is less compared to female donors. Also, the average fibrillar collagen content in donors above 65 years of age was higher compared to those below 65. However, both differences were not statistically significant. Interestingly, ex-smokers have significantly more fibrillar collagen content compared to actively smoking donors (Figure S5Cii). Although interesting, the underlying mechanisms for these differences remain elusive.

hPCLS show variable response of fibrillar collagen deposition upon TGFß1 stimulation:
hPCLS derived from the lung parenchyma of non-ILD patients were stimulated with TGFß1 and culture supernatants were harvested on day 13 of *ex vivo* culture. The supernatants were subjected to ELISA measurements for PRO-C1 and FBN-C (Figure 6A i-ii). The data shows an unequivocal upregulated synthesis of both markers upon TGFß1 stimulation across all the donors (n=10). To analyse if the upregulated synthesis of ECM proteins (Figure 4B) and PRO-C1, FBN-C (Figure 6A i-ii) results in a corresponding increase in ECM deposition, we employed our label-free SHG imaging and image analysis pipeline to quantitatively measure the deposition of fibrillar collagen in unstimulated and TGFß1 stimulated hPCLS (derived from tissue resection of non-ILD patients). The raw values of SHG intensity (iSHG) of interstitial ROIs from vehicle and TGFß1 stimulated hPCLS values were log2 transformed (Log2iSHG), normalised to the mean SHGintensity (Log2iSHGc) of each donor (3-6 hPCLS/ donor, 18 donors). In contrast to the consistent elevated levels of PRO C-1 and FBN-C as determined by ELISA measurements, Log2SHGi values of fibrillar collagen shows no significant additional deposition of fibrillar collagen (Figure 6Bi) in the interstium of hPCLS stimulated with TGFß1 in comparison to control tissue (Figure 6C, FigureS5D). Interestingly, differential proteomic analysis of vehicle and TGFß1 stimulated hPCLS (day 13, Table S4) showed that some of the metalloproteinase specific for degradation of native collagens (Type I, II, III, IV, V, VII, X, and XI)[30], also known as collagenases, such as MMP2 (Log2FC 0.68), MMP3 (Log2FC 0.65) & MMP14 (Log2FC 0.52) showed upregulation in our *ex vivo* culture system after TGFß1 treatment, while MMP12 (Log2FC -0.97) and MMP9 (Log2FC -1.2) were downregulated. These data are consistent with recent data in murine models of PCLS, where collagen type I, III and elastin have been shown to have high turnover due to higher MMP activity[50]. Also, Han S. et al.[51] has shown that pan inhibition of MMP activity using Ilomastat (GM6001) enhances collagen fibril formation in human mesenchymal stem cells in *in vitro* cultures.

Metalloproteinase (MMP) inhibitor together with TGFß1 stimulation significantly enhances deposition of fibrillar collagen in ECM.
Next, keeping in view the observed differential upregulation of different MMPs in ex vivo culture of hPCLS (Figure 3), as stated above (Table S4), and reports that imbalance of MMP activity is crucial to fibrotic tissues[52], 14 donors were additionally treated with a combination of TGFß1 and GM6001 (MMPi). Out of these 14 donors, for 7 media supernatants were collected on day 13. ELISA analysis of hPCLS conditioned supernatants was performed for PRO-C1 and FBN-C (Figure 6 iii-iv).

The results showed that MMPi treatment alone (4 donors) has no effect on the synthesis of these markers. TGFß1 stimulation expectedly resulted in consistent upregulation of both these markers compared to unstimulated hPCLS supernatants. Interestingly, concomitant stimulation of TGFß1 and MMPi resulted in an increased amount of both PRO-C1 and FBN-C compared to TGFß1 treatment alone (Figure 6 iii-iv). Next, to investigate whether treating hPCLS with TGFß1+MMPi results in an increased deposition of fibrillar collagen in lung ECM, vehicle, MMPi, TGFß1, and TGFß1+MMPi stimulated hPCLS were analysed by our SHG workflow.
MMPi treatment alone had no statistically significant effect on the interstitial collagen SHG signal compared to respective vehicle-treated hPCLS (Figure 6B ii). Concomitant treatment of TGFß1 and MMPi resulted in significantly more deposition of fibrillar collagen compared to TGFß1 treatment alone (Figure 6B ii). Patient-specific analysis of the data (Figure 6B iii) showed that in some patients, TGFß1 treatment caused a decrease and in others, an increase in SHG signal compared to control hPCLS. Although very interesting, the reasons for this differential response to TGFß1 treatment are currently unclear. However, for every sample analysed, concomitant treatment with MMPi resulted in consistently higher fibrillar collagen signal compared to TGFß1 treatment alone. Together these data confirm that metalloproteinase expression/ activity is a rate-limiting factor in the hPCLS model system characterised here for deposition of fibrillar collagen upon TGFß1 stimulation.

Discussion:

hPCLS have emerged as a model system with high potential for recapitulating pathophysiological conditions close to that of human physiology[10,18]. However, a characterisation of the inherent molecular changes that such a system undergoes in *ex vivo* culture has not been reported to date.
In this study, we report for the first time proteomic and metabolomic changes of the hPCLS over two weeks of ex vivo culture. This is significantly longer than the 7 days previously reported[10,18]. These cell-type data (Figure S2C) was derived from curation of our phenotypic protein expression data to that of RNA-seq data available in the LGEA database. Comparison of the LGEA database sequencing list and recently published single cell sequencing results of human lung tissue[53–55] shows that some markers classified in the LGEA database as cell-type specific are actually present in more than one cell sub-type (e.g.TAGLN, ACTA2, PDGFRA)[55]. Nonetheless, we show that proteins exclusively expressed in the four major cell types[25] of lung tissue are present after two weeks of *ex vivo* culture (Figure S2C). Interestingly, the data also reveal (Figure 3 and Figure S2B) the presence of a persistent ECM degradative inflammatory activity during the 2 weeks of *ex vivo* culture, which is assumed not to be present under healthy physiological conditions. This finding challenges the general assumption in the field that physiologically healthy conditions are preserved in *ex vivo* culture of hPCLS[20]. The source of this inflammation activity is currently unclear. One explanation could be that it occurs due to sample preparation, specifically, tissue slicing. Alternatively, it cannot be excluded that the occurrence of the degradative inflammatory activity results from the fact that the tissue slices used in our study are derived from tumor adjacent areas which have previously been shown to be immunologically active[56]. The observation that these changes occur mainly during the first 4 days in culture, it may be advisable in future studies to start investigations after this “stabilizing period”. However, our studies show that there is already loss of protein expression in lung cell markers, such as SFTPC and AGER within the first 4 days of culture. Therefore, depending on the question addressed,

we consider it important to compare results obtained in the “stabilizing period” with the first 4 days of culture. Furthermore, It would also be interesting to test if treating hPCLS with cell culture levels of Hydrocortisones might be useful to prevent this inflammatory activity.

The presence of cell types such as epithelial, endothelial and immune cells (Figure S2C) suggests the possibility of transition of these cell types into myofibroblasts upon stimulation with cytokines such as TGFß1[3], hence eliciting a physiologically relevant pro-fibrotic response. Consistent with other studies[10], our proteomic analyses showed after TGFß1 treatment upregulation of many pro-fibrotic markers (Figure 4A-B) including pro-fibrotic fibrillar collagens COLI, COLIII and COLV. On day 13 of hPCLS ex vivo culture, a total of 109 proteins were significantly upregulated. Strikingly, 64 out of 65 upregulated proteins are characteristic of mesenchymal cell-type, and 40 out of 44 downregulated genes are specific to epithelial cell-type (Figure S4C). These data suggest that the pro-fibrotic signal induced after TGFß1 treatment of hPCLS might be due to an epithelial to mesenchymal transition (EMT)[3]. Alternatively, the downregulation of epithelial proteins with a concomitant increase in mesenchymal markers could also be epithelial cell death or simply impairment of epithelial genes with a concomitant increase in mesenchymal markers in mesenchymal cells. However, to establish this hypothesis further, complementary analyses such as single cell RNA sequencing could be used. Importantly, these experiments are now facilitated due to recent advances in single cell and high quality RNA preparation from hPCLS[57]. Furthermore, to visualise the dynamics of single cell types in hPCLSs and test if they are consistent with our proteomics data, our live imaging set-up can be coupled to that of Akram et al[20].

Other studies[10,18] have used hPCLS for studying fibrotic signalling; however, a readout that measures extracellular matrix deposition during the ex vivo culture has been lacking. Similarly, in other model systems, only indirect readouts such as ELISA[58] of pro-collagen peptides or hydroxyproline levels in serum have been used to infer on fibrosis, e.g. in liver, kidney or lung[59–61]. In the hPCLS model system, collagen has been qualitatively monitored using antibodies and immunohistochemistry approaches[18]. However, the antibodies used in these studies could not discriminate between fibrillar and non-fibrillar collagen types. In order to overcome these limitations, we applied label-free second harmonic imaging to specifically quantify the fibrillar collagen content present in the ECM of hPCLS. A key advantage of label-free imaging is its ability to image deep into the tissues and specifically measure fibrillar ECM deposited collagen. SHG imaging analysis of non-ILD and ILD patient-derived hPCLS, showed higher levels of fibrillar collagen in ILD derived hPCLS compared to tissues from non-ILD donors (Figure 5B-C), showing the quantitative nature of the imaging workflow established here. Our image analysis shows that documenting interstitial collagen levels as a function of age, gender, smoking status (Figure S5C i-iii) together with other lung vitals could prove to be a powerful tool to detect susceptibility to ILD in humans. And this can be combined with other molecular techniques to pin down underlying causes, therefore giving novel insights into the disease mechanism. Interestingly, the increased expression of pro-fibrotic markers in TGFß1 stimulated hPCLS COLI (PRO-C1-ELISA, COL1A2-proteomics), as revealed by our ELISA and proteomics analyses, did not result in a corresponding significant increase of deposition in ECM (Figure 6B). This observation could possibly be explained by differential regulation of MMPs and their respective enzymatic activities in non-ILD patient-derived hPCLS upon TGFß1 treatment (Table S4). Here, we observe that MMP9 and MMP12 are significantly

downregulated, these two MMPs might have immune response-related role in hPCLS as both these enzymes have been described to regulate shedding of CD14 receptor to influence innate host defense[62] . The only detected tissue inhibitor of metalloproteinase, TIMP3 showed no significant change. On the other hand, MMP2 and MMP14, are upregulated (Table S4). The later have been known to have COL I, II and III as substrate[30], therefore, in this case, upregulation might result in enhanced COL degradation before deposition[30]. In support of this hypothesis concomitant treatment with TGFß1 and GM6001, an MMP inhibitor, increased the levels of PRO-C1 and FBN-C (Figure 6iii-iv) in conditioned supernatants, and increased fibrillar collagen deposition in comparison to TGFß1 treatment alone. These data underline, consistent with existing literature, the importance of MMP activity for fibrillar collagen deposition and thus the development of fibrosis. As GM6001 is a broad MMP inhibitor, more experiments will be necessary to dissect which MMP(s) in particular participate in this process. It would also be interesting to investigate the effect on fibrillar collagen deposition quantitatively by stimulating hPCLS with cocktails of pro-inflammatory molecules as it has been successfully demonstrated qualitatively by Alsafadi et al[18].

Pulmonary fibrosis is essentially an ageing related disorder[63] developing over several years. Therefore, increases of fibrillar collagen deposition within two weeks can be expected only to be modest, as observed here. However, we show that concomitant treatment with TGFß1 and MMPi, enables the measurement of enhanced fibrils deposition in response to TGFß1 treatment in this *ex vivo* model system demonstrating the potential of our integrated approach developed here. Interestingly, not all patients' samples responded equally to TGFß1 (Figure 6B, FigureS5D). Out of the 18 donors tested, 2 showed no difference, 8 donors showed an increased, and surprisingly 8 showed a decreased signal upon TGFß1 treatment (Figure 6B, FigureS5D). Dividing the response of the donors according to their gender, smoking status and age (Figure S5D-E) did not reveal any obvious factor that might explain these variations in TGFß1 response. Therefore, it remains unclear why different patients respond differently to TGFß1 treatment. One explanation could be that certain hPCLS are more predisposed for ECM deposition than others due to their spatial origin in the lung. Tissue spatial variation of developing fibrotic foci has been reported to be a characteristic of pulmonary fibrosis development[64]. We can therefore not exclude the possibility that the variations of SHG signal in response to TGFß1 treatment is caused by such spatial variations. We can also not exclude the possibility that the variability in TGFß1 activity is due to variations in stiffness[65,66] of the ECM of hPCLS.

Our multiomic characterisation of hPCLS show that they are metabolically viable, and contain all lung relevant cell types up to two weeks in ex vivo culture. These data support the idea that these hPCLS model system can be used to study human lung physiology related molecular processes. However, apparent limitations exist. Our proteomic analysis shows that hPCLS in culture undergo significant changes in MMPs, collagens and pro-inflammatory pathways. This is in contrast to what has been proposed or assumed in earlier studies[67] lacking such multiomic analyses. Recent studies show that after onset of the disease, e.g. initial fibroblast activation and ECM accumulation, recruitment of circulating immune cells further enhancefibrosis[68]. In the hPCLS model system, these cells do survive, but their constant replenishment as it occurs in the human body is still missing. Addition of these circulating cell from the same donor to the hPCLS culture at different days would be a powerful tool to establish their role in fibrosis progression. Furthermore, physiological aspects of lung compliance such as cycling oxygen levels and changes

in mechanical tension are also lacking. A key addition to improve the current experimental culture setup could therefore be to culture hPCLS in a bioreactor system that mimics these important components of lung physiology.

Anonymised Patient Id	Age (Years)	Gender	Smoking Status	Disease Diagnosis	Tissue used

IPF lungs develop fibrotic foci, rather than diffuse fibrosis, which have been extensively characterised by Jones et al.,[64]. The image analysis approach developed here focuses on interstitium of lung parenchyma and could in the future help to identify the progression and development of such foci in a quantitative manner. We propose that the complementary approach described here, using label-free imaging of hPCLS together with the measurement of soluble markers such as PRO-C1, FBN-C, C3M, could enable the characterisation of the dynamics of collagen synthesis and degradation (the fractional synthesis) *ex vivo* upon fibrosis progression. Furthermore, to dissect the role of single cell types in mediating the effects of various pro-fibrotic stimuli, our workflow could be coupled to the newly established single cell analysis pipeline in hPCLS by Stegmayr et al[57].
Also, as SHG does not require sample fixation, as it is the case for immunochemistry, this label-free approach should allow time-lapse studies monitoring the kinetics of ECM deposition over extended periods of time. Initial proof of concept experiment has shown the feasibility of this approach (Figure S6). Live SHG imaging will allow to assess the kinetics of fibrillar collagen deposition as well as regression, upon therapeutic or pharmacological intervention.
In summary, our SHG imaging set-up and analysis pipeline established here will be a powerful tool for studying fibrosis in the future.

Acknowledgements:
Technical assistance of Christa Stolp from Biomaterial Bank Heidelberg (BMBH) in tissue assembling is gratefully acknowledged. We would also like to acknowledge the help of Vikki Barrett (GSK Stevenage) for help in training with Krumdieck. We sincerely thank Katrin Strohmer and Anna Rutkowska-Klute (Cellzome-GSK) for their help in setting up the SHG imaging. Pepperkok team and all the EMBL core facilities are also acknowledged for their support, manuscript preparation and fruitful discussions for data analysis.

Funding: The research was funded by a joint EMBL-GSK postdoctoral programme and by the German Centre for Lung research (DZL)

LT04	66	F	S	Adenocarcinoma	Resection
LT05	68	M	S	Squamous cell carcinoma	Resection
LT06	78	F	ES	Squamous cell carcinoma	Resection
LT07	50	M	ES	Adenocarcinoma	Resection
LT08	63	M	S	Squamous cell carcinoma	Resection
LT13	48	M	N	Metastasis	Resection
LT18	67	F	S	Adenocarcinoma	Resection
LT19	60	F	ES	Carcinoma	Resection
LT21	56	F	S	Adenocarcinoma	Resection
LT22	75	F	ES	Adenocarcinoma	Resection
LT24	68	M	ES	Squamous cell carcinoma	Resection
LT25	65	M	N	Neuroendocrine Tumor	Resection
LT30	77	F	ES	Adenocarcinoma	Resection
LT31	65	M	ES	Squamous cell carcinoma	Resection
LT32	68	F	ES	Squamous cell carcinoma	Resection
LT35	69	M	ES	Adenocarcinoma	Resection
LT36	62	M	ES	Squamous cell carcinoma	Resection
LT37	63	F	S	Adenocarcinoma	Resection
LT38	67	M	S	Non-small-cell lung carcinoma	Resection
LT39	67	F	S	Non-small-cell lung carcinoma	Resection
LT40	68	F	N	Adenocarcinoma	Resection
LT44	68	M	S	Squamous cell carcinoma	Resection
LT62	50	M	ES	Carcinoma	Resection
LT63	67	M	ES	Adenocarcinoma	Resection
LT139	69	M	S	Adenocarcinoma	Resection
L340	62	M	ES	IPF	Transplant Recipient
L348	59	M	ES	IPF	Transplant Recipient
L324	59	M	S	NSIP	Transplant Recipient
L323	58	M	N	IPF	Transplant Recipient
L315	56	M	N	IPF	Transplant Recipient
ET01	68	M	ES	Squamous cell carcinoma	Resection
ET02	68	F	N	Adenocarcinoma	Resection
ET03	57	F	N	Adenocarcinoma	Resection
ET04	65	F	ES	Adenocarcinoma	Resection
ET05	70	F	ES	Squamous cell carcinoma	Resection
ET06	57	M	ES	Squamous cell carcinoma	Resection

Table 1: Patient information:

M= Male; F= Female; S= Active Smoker; N= Never Smoked; ES= Ex-Smoker; IPF= Idiopathic Pulmonary Fibrosis; NSIP= Nonspecific interstitial pneumonia; Resection= Tumor Free lung tissue (non-ILD patients) from an area distant to lung tumor tissue resected; Transplant Recipient= Fibrotic Lung Tissue from Fibrosis patients receiving a transplant

Table 2: Log Normality test values for SHG intensity comparison of Untreated hPCLS (Day 13):

Anderson-Darling test	Whole hPCLS	ROI hPCLS
A2*	0.9273	0.3467
P value	0.0176	0.4716
Passed normality test (alpha=0.1)?	No	Yes
P value summary	*	ns
D'Agostino & Pearson test		
K2	5.067	1.434
P value	0.0794	0.4882
Passed normality test (alpha=0.1)?	No	Yes
P value summary	ns	ns
Shapiro-Wilk test		
W	0.9520	0.9835
P value	0.0080	0.4784
Passed normality test (alpha=0.1)?	No	Yes
P value summary	**	ns

Figure Legends:

Figure 1: Schematic representation of the experimental workflow: (A) 1-3. On day 0, tumor free tissue (distal to tumor site) from resection of non-interstitial lung disease patients (non-ILD) is surgically removed and classified as tumor free by the local pathologist. 4. Tumor free tissue is received and inflated with 3% low melting agarose. 5. Tissue cores of varying heights are prepared. 6. Precision cut lung slices (hPCLS) of 8mm diameter and 250µm thickness are prepared using Krumdieck tissue slicer. On day 0, each hPCLS generated is distributed across a 24 well plate (1 hPCLS/ well). For all the days of culture, each hPCLS is cultured in 750µl of DMEM with constant presence of anti-microbials (Amphotericin B and Pen-Strep). From day 0 to day 1 (18 hrs), the tissue is kept in DMEM with 10%FCS. (B) 7. On day 1, old media (with FCS) is replaced with fresh media (No FCS). Media (with no FCS) is also replenished on day 4, 7, & 10. Here, when required hPCLS are additionally treated with TGFß1 or any other stimulant from day 1 onwards. 8. On day 13, hPCLS are harvested for downstream SHG analysis and proteomics (involving TGFß1 stimulation).
‡ we have used 5 ILD patients' derived hPCLS as well, PFA fixed directly on day 0, but only for SHG analysis (non-ILD vs ILD) ‡‡ For ILD patients the tissue is taken from lung parenchyma of transplant recipeint patients. ‡‡‡ hPCLS treated with DMEM containing 10% FCS only for first 18 hrs of culture. # In experiments involving ELISA measurements, old media supernatants (day4, 7 & 13) from each hPCLS (±TGFß1) is collected separately and subjected to soluble marker measurements. ## For proteomics and metabolomics of hPCLS without any treatment, slices were also harvested on day 1, 4, 7, 10 in addition to day 13 while as for live-imaging viability analysis on day 1, day 7 and day 13.

Figure 2: Multiomic analysis of molecular changes in *ex vivo* cultured hPCLS: hPCLSs derived from tissue resections of non-ILD patients (4 donors) in *ex vivo* culture was harvested on day 1, 4, 7, 10 and day 13 without any treatment and were subjected to mass spec analysis. (A) Volcano plot analysis of the proteome of hPCLS cultured ex vivo over time. Log2FC of the respective proteome on a given day of culture was normalised to the previous time point. Analysis highlights that hPCLS undergo moderate changes in the first few days of culture and remain stable over time. (B) Untargeted metabolomic analysis of hPCLS was performed. Volcano plot analysis of log2FC changes in ions was performed similarly as above. The analysis confirms that hPCLS undergo very moderate metabolic changes similarly as the proteome changes. Donor ids: LT21, LT22, LT24 and LT25. 2 replicates/ donor, 2 hPCLS/ replicate. Table S6: donor centric breakdown of mass spec data

Figure 3: Differential regulation of metalloproteinases (MMPs) and collagens (COL) upon *ex vivo* culture of hPCLS: The heat map shows the Log2 fold changes in the levels of MMPs and different COLs detected in the proteomics analysis of unstimulated hPCLS over time in *ex vivo* culture. The Log2 fold changes are calculated with respect to day 1. * fdr p values, fdr < *0.05, <0.01**, <***0.001.

Figure shows a consistent upregulation of ECM degrading, remodelling signalling network with reduced levels of COLs as well.

Figure 4: Assessment of pro-fibrotic signalling induction upon TGFß1 stimulation of *ex vivo* cultured hPCLS (derived from tissue resection of non-ILD patients): (A) ELISA analysis of media supernatants of vehicle and TGFß1 treated hPCLS (4 hPCLS/ donor). Color of each dot represent different donors and the number of dots represent each hPCLS. Media supernatant on different days was collected from each hPCLS. Absolute concentration (in ng/ml) were determined (TableS8). Here, all the values were normalised to the mean vehicle-treated control (of each donor) on day 4. PRO-C1, FBN-C peptide and C3M soluble pro-fibrotic markers were analysed. 4 media supernatants (each from a hPCLS derived from respective donor) were analysed over time. Results show clear upregulation of majority of these markers. ELISA data was statistically analysed using a simple one-way annova, ANOVA with Turkey's multiple comparisons test. Shapiro-Wilk normality test confirmed data normality. Donor ids: LT08, LT13 and LT18 (B) TGFß1 and vehicle-treated hPCLS were harvested on day 13 of *ex vivo* culture. Log2FC of proteins shown to involved fibrotic signalling upon TGFß1 stimulation on day 13 (with respect to vehicle day 13) of hPCLS culture is shown here. Proteomics data p-values represent false discovery rate. *p<0.05, **p< 0.01***p<0.001. Donor ids: LT21, LT22, LT24 and LT25. 2 replicates/ donor, 2 hPCLS/ replicate. Table S7: donor centric breakdown of mass spec data

Figure 5: Second Harmonic generation image analysis of fibrillar collagen in hPCLS: (A) The scheme represents the SHG microscopy and imaging setup. hPCLS are imaged in a 3D tiled scan with a 20X air objective. (B-C) Maximum Z-projection and quantification of SHG z-stacks of PFA fixed (day 0) hPCLS from non-ILD and ILD patients. Violin plots show Log2SHGi-normalised values. In a two-way annova performed here, disease type and donor to donor variation were used as factors ***p<0.001. Same Coloured dots represent a donor. Here, 4 non-ILD donor derived hPCLS (3-4 hPCLS/ donor) and 5 ILD donor derived hPCLS (3-4 hPCLS/ donor) were used. Donor ids non-ILD patients: LT04, LT05, LT06 and LT07; ILD patients L340, L348, L323, L324, L315 (D) SHG images of hPCLS from a non-ILD donor tissue resections that were cultured for 13 days and PFA fixed. Donor Ids: LT08, LT13, LT18, LT19, LT35, LT36, LT37, LT38, LT39, LT40, LT44, LT139, ET01, ET02, ET03, ET04, ET05, ET06 (E) Semi-automated FIJI based script divides the SHG 3D image stack of hPCLS into 8x8 grids (approx. 0.8X0.8mm). Magenta "X" represents the example rois that excluded from the analysis. Workflow for quantifying SHG signal originating from lung interstitium. Forward and backward SHG channel intensity is added and total fibrillar collagen is calculated. (F) Color of the points in the plots represent hPCLS/ donor. Graph shows that whole hPCLS SHGintensity values are more variable then the interstitial ROIs from the same donor pool. Scale bar 1000 µm.

Figure 6: Second harmonic generation image analysis of fibrillar collagen deposition in *ex- vivo* cultured hPCLS upon stimulation with TGFß1 and TGFß1+metalloproteinase inhibitor (MMPI). [A(i-ii)] Relative amount of PRO-C1 and FBN-C in the supernatants of vehicle and TGFß1 stimulated hPCLS. Coloured dots represent different donors and the number of dots represent each hPCLS. Media supernatant on different days was collected from each hPCLS supernatant. Absolute concentration (in ng/ml) were determined (TableS9). The results show consistent upregulation of both PRO-C1 and FBN-C upon TGFß1 stimulation across all donors. All the values were normalised to the mean vehicle-treated control (of each donor) on day 13. In total 10 donors (donor ids- LT08, LT13, LT18, LT35, LT36, LT37, ET01, ET02, ET03, ET04). [A(iii-iv)] Relative amount of PRO-C1 and FBN-C in the supernatants of vehicle, MMPi, TGFß1 and TGFß1 stimulated hPCLS. Absolute concentration (in ng/ml) were determined (TableS10). All the values were normalised to the mean vehicle-treated control (of each donor) on day 13. In total 7 donors (donor ids- LT35, LT36, LT37, ET01, ET02, ET03, ET04). (Bi) The raw values of SHGintensity(iSHG) of interstitial ROIs from vehicle and TGFß1 stimulated hPCLS values were log2 transformed (Log2iSHG) normalised to the mean SHGintensity (Log2iSHGc) of each donor (unlike global normalization) (3-6 hPCLS/ donor, 18 donors). Results (Log2SHGi) show no significant difference in deposited fibrillar collagen upon TGFß1 stimulation. (B ii-iii) Log2SHGi values of fibrillar collagen in hPCLS upon vehicle, MMPi, TGFß1 and TGFß1+MMPi treatment. (B iii) mean Log2SHGi of each donor in response to vehicle, MMPi, TGFß1 and TGFß1+MMPi treatment. Results show significant increase in fibrillar collagen signal upon TGFß1+MMPi treatment. Each line connects the response of same donor(C) Maximum Z-projection of representative rois of vehicle, TGFß1 and TGFß1+MMPi (MMPI) treated hPCLS (same donor). Scale bar 250µm. Two-way annova (with treatment and donor as two variables) Turkey's multiple comparisons test was performed, *p<0.05, **p< 0.01***p<0.001. Shapiro-Wilk normality test

confirmed data normality. For vehicle, TGFß1, TGFß1+MMPi stimulated hPCLS 14 donors were analysed with 3-6 hPCLS/ donor, while as for MMPi only 7 donors were analysed. Donor Ids: LT08, LT13, LT18, LT19, LT35, LT36, LT37, LT38, LT39, LT40, LT44, ET01, ET02, ET03, ET04, ET05, ET06.
NOTE: The ELISA data from donors LT08, LT13, LT18, LT35, LT36, LT37 on day 13 is the same as in Figure 4A and 6Aiii-iv. The data is reused in this figure to represent unequivocal upregulation of PRO-C1 and FBN-C across all donors.

Figure S2: (A) Representative live confocal images (20X air objective) of hPCLS incubated with Calcein AM (labels live cells) and Ethidium homodimer (Dead cells) and quantification live tissue (Calcein signal) and dead cell count (ethidium homodimer) Error bars represent SEM, and p-values were calculated using ordinary one-way ANOVA, **p<0.001. Note each hPCLS was imaged only once during ex vivo culture. 3 hPCLS were analysed per day from 3 donors over all. Each dot represents a field of view imaged (5-6 fields of view were imaged/ hPCLS/ day). Scale bar 250µm (B) Significantly regulated genes on day 13 compared to day 1 were subjected to Cytoscape pathway analysis. The number of genes in each enriched GO terms present in our data set was plotted. Term Pvalue represents the pvalue for association of these genes to whole of GO term. % associated genes, is the percentage of our genes overlapping with all of the members of a given GO term. (C) Significantly regulated genes (day 13 vs. Day 1) were compared with unique cell type markers as established in LGEA[25] study. A, B, C and D mark comparisons of day4 vs day1, day7 vs day1, day10 vs day1 and day13 vs day1 respectively. Commonly used lung cell-type markers detected in our proteomics set-up (D) Volcano plots show Log2FC of all the genes detected against their respective fdr. Red dots represent highly significant genes, while as blue are those regulated that are significant but moderate in the level of change. (E) Metabolites detected upon LC/MS were similarly plotted as in (D). (F) Represent individual metabolites and their change over days in *ex vivo* culture. (G) ATP level measured using ATP glo assay. Coloured dots represent hPCLS from the same donor.

Figure S4: (A) List and Log2FC level of significantly regulated genes upon TGFß1 treatment compared to unstimulated (day 13) (B) Pathway analysis of significantly regulated genes upon TGFß1 treatment compared to unstimulated hPCLS (day 13). The analysis was carried out using Cytoscape. (C) Significantly regulated genes were compared to different cell-type markers as established by LGEA[25] study and log2FC were plotted as a heat map.

Figure S5: (A) Raw SHGintensity values of whole hPCLS from non-ILD patients and ILD patients. #, non-ILD SHGintensity values plotted on a different scale (B) Raw SHGintensity values of whole hPCLS from all 18 donors (unstimulated condition, 3-6 hPCLS/ donor). Color of the dots represent same donor. (Ci) Log2SHGi values of interstitial collagen (ROI analysis) to the amount of interstitial fibrillar collagen in vehicle-treated hPCLS on day 13. Upon global normalization (to mean of all donors), data shows below average fibrilar collagen amounts in male interstitium. (Cii) Log2SHGi values show that ex-smoker donors have significantly more interstitial collagen. (Ciii) Log2SHGi values show that donors grouped in age group equal to or above 65 years also show above average interstitial fibrillar collagen. Significance was calculated using one-way annova (*p value< 0.05). Donor id: All vehicle-treated donors from Figure 6 Bi. (D-E) Gender, smoking status and age specific breakdown of Log2SHGi values of fibrillar collagen of donors upon vehicle and TGFß1 treatment.

Figure S6: (A) Maximum projection images of 2-photon excited autofluorescence from the same hPCLS on different days shows that we can reliably find the same regions. Representative SHG images of hPCLS show that selective regions of hPCLS have increased fibrillar collagen deposition upon TGFß1+MMPi treatment (white asterisks). B-C) Quantification of raw SHG values of hPCLS with only vehicle treatment (unstimulated) and, D-E) TGFß1+MMPi treatment. B & D) Raw SHG intensity values on day 01 and day 13 in untreated and TGFß1+MMPi treated hPCLS respectively. C & E) Day 01 normalised values on day 01 and day 13 in untreated and TGFß1+MMPi treated hPCLS respectively. E) Day 1 normalised SHG values on day 13 show an increase in SHG signal upon TGFß1+MMPi treatment for 2 weeks. F) Representative ROIs showing increased fibrillar collagen deposition (ROIs are zoomed asterisk marked region of Figure S6A SHG channel). Different colors represent different donors. Donor Ids: LT62, LT63. Scale bar 500µm. Note: For Untreated condition, only 1 hPCLS was analysed for LT62 donor.

Materials and methods:

Lung resection supply and licenses:

Throughout this manuscript, all the hPCLS that were cultured *ex vivo* were derived from lung tissues resected from tumor free areas (in total 26 donors). A list of all the donors used in this study with their age, gender, smoking status, major clinical diagnosis and the experiments used in are listed as a in Table 1. Tumour-free tissue from human lung tissue resections of lung cancer patients were obtained from Thoraxklinik-Heidelberg with anonymized patient Ids. The tumor-free tissue is selected by the pathologist during tissue resection. The patient consent and use of tissue was obtained as per the research ethics committee (Medical Faculty of University Heidelberg) approval reference number S-270/2001. Apart from tissue resections, we have also used samples belonging to ILD patients. In total we used 5 ILD patient sample. Details of these samples have also been added to Table Patient information. The tissue used to generate hPCLS is a section of ILD lung parenchyma, (tissue from lungs transplant recipient was used). The fibrotic foci aren't visible during the processing procedure; therefore, it is not possible to say that the individual slices generated for each donor contained fibrotic foci. Samples of ILD lung tissue were obtained from patients undergoing lung transplant for end–stage disease from Institute of Transplantation, Newcastle Upon Tyne Hospitals. The patient consent and use of ILD tissue was approved by national research ethics service (11/NE/0291) and UK Health Research Authority. The human biological samples were sourced ethically and their research use was in accord with the terms of the informed consents under an IRB/EC approved protocol.

Precision-cut lung slice preparation and *ex vivo* culture:
Non-ILD and ILD hPCLS were prepared as described previously[69,70]. Briefly, on the day when the tissue resection was received (day 0), lung tissue was inflated with 3% low melting agarose (Sigma#A9414) prepared in phenol free DMEM (Gibco# 41965-039). Next, 8 mm cores were prepared and 250 µm thick slices were generated using a Krumdieck tissue slicer. To facilitate recovery following the slicing procedure, tissue media was supplemented with penicillin, streptomycin, fungizone and 10% FCS for the first 18 hrs of ex vivo culture. After 18 hrs, next day (day1), the media (± stimulation) was replenished and henceforth after every 72 hours till day 13. Cell culture grade plastic 24 well plates (Greiner#353226) were used to culture hPCLS. On day 0 media was additionally supplemented with 10% FCS (Gibco#10270106). The hPCLS were treated with 10ng/ml recombinant human TGFß 1 protein (R&DSystems#240-B-010) and 25µM (in 750µl of DMEM) of MMPI (Merck#CC1010). Live dead staining was carried out using calcein-am/ ethidium homodimer kit (ThermoFisher#L3224) as per supplier recommendations. The hPCLS were incubated in recommended concentration of live/dead reagents for 45 minutes prior to live confocal microscopy. hPCLS were always cultured in presence of penicillin-streptomycin (Gibco# 15140122) and amphotericin B (Giboc#15290026).

ELISA measurements:
Soluble extracellular matrix fragments (PRO-C1, FBN-C, C3M) were determined in the media supernatant by competitive (ELISA) assays developed and validated by Nordic Bioscience A/S (Herlev, Denmark). According to the manufacturer's instructions[35 71 72]. Values measured below the detection limit of the assay were assigned the lower limit of detection (LLOD).

Mass spectrometry sample preparation and analysis:

Proteomics:
Briefly, hPCLS were washed with PBS and harvested using snap freezing in liquid Nitrogen. Upon thawing, samples (2 hPCLSs/technical replicate) were dissolved in 300µl of 2% SDS-H_2O (with protease and phosphatase inhibitor) for 2 hours at room temperature. Subsequently, mechanically homogenised using bead ruptor. Before LC-MS/MS analysis, protein concentrations were measured (Pierce 660nm kit# 22660). Next samples were solubilised in 2 × SDS sample buffer and subjected to short SDS gel electrophoresis. Samples were further processed for LC-MS/MS analysis.
SDS PAGE gels were Coomassie stained. Gel lanes were cut into three slices covering the entire separation range (~2 cm) and subjected to in-gel tryptic digestion[73]. Peptides were labeled via isobaric mass tags (TMT10, Thermo Fisher Scientific, Waltham, MA).TMT labeling was performed using the 10-plex TMT reagents, enabling relative quantification of 10 conditions in a single experiment[74]. Briefly, the labeling reaction was performed in 40 mM triethylammonium bicarbonate, pH 8.53 at 22°C and quenched with glycine. Labeled peptide extracts were combined to a single sample per experiment. Lyophilized samples were re-suspended in 1.25% ammonia in water and subjected to LC-MS/MS[74].

Peptide and protein identification & identification
Mascot 2.4 (Matrix Science, Boston, MA) was used for protein identification by using a 10 parts per million mass tolerance for peptide precursors and 20 mD (HCD) mass tolerance for fragment ions. The search database consisted of a customized version of the International Protein Index protein sequence database combined with a decoy version of this database created by using scripts supplied by MatrixScience.
Reporter ion intensities were read from raw data and multiplied with ion accumulation times (the unit is milliseconds) so as to yield a measure proportional to the number of ions; this measure is referred to as ion area [75]. Spectra matching to peptides were filtered according to the following criteria: mascot ion score > 15, signal-to-background of the precursor ion > 4, and signal-to-interference > 0.5 [75]. Fold changes were corrected for isotope purity as described and adjusted for interference caused by co-eluting nearly isobaric peaks as estimated by the signal-to-interference measure [75]. Protein quantification was derived from individual spectra matching to distinct peptides by using a sum-based bootstrap algorithm; 95% confidence intervals were calculated for all protein fold changes that were quantified with more than three spectra [75].

Metabolomics:
hPCLSs were snap-frozen on the day of harvest. On the day of sample preparation, 2hPCLS/ technical replicates were shortly rinsed in 75mM Ammonium bicarbonate (pH 7.4) and mechanically homogenised in MS grade H_2O to extract metabolites. Untargeted metabolomics analysis was performed as described[76]. Briefly, samples were analysed on a LC/MS platform consisting of a Thermo Scientific Ultimate 3000 liquid chromatography system with autosampler temperature set to 10° C coupled to a Thermo Scientific Q-Exactive Plus Fourier transform mass spectrometer equipped with a heated electrospray ion source and operated in negative ionization mode. The isocratic flow rate was 150 µL/min of mobile phase consisting of 60:40% (v/v) isopropanol: water buffered with 1 mM ammonium fluoride at pH 9 and containing 10 nM taurocholic acid and 20 nM homotaurine as lock masses. Mass spectra were recorded in profile mode from 50 to 1,000 m/z with the following instrument settings: sheath gas, 35 a.u.; aux gas, 10 a.u.; aux gas heater, 200° C; sweep gas, 1 a.u.;

spray voltage, -3 kV; capillary temperature, 250° C; S-lens RF level, 50 a.u; resolution, 70k @ 200 m/z; AGC target, $3x10^6$ ions, max. inject time, 120 ms; acquisition duration, 60 s. Spectral data processing was performed using an automated pipeline in R as described previously[76]. Detected ions were tentatively annotated as metabolites based on matching accurate mass within a tolerance of 5 mDa using the Human Metabolome database[77].

Data analysis:

Proteomics: The R programming language (ISBN 3-900051-07-0) was employed to process the proteins output files of IsobarQuant. Only proteins which were quantified with at least two unique peptides and which were quantified in all experiments were used for further analysis. The "sumionarea protein" columns were annotated to different experimental conditions. Then, potential batch-effects were removed using the limma package[78] and the results were normalised using the vsn package[79]. Limma was also used to test for differential expression of proteins. A protein was considered significant with a 2-fold difference and a false discovery rate below 5 %. All significant proteins were clustered (hierarchical clustering – ward.d2 method) based on their Euclidean distances of log2 ratios towards the respective control.

Network analysis using Cytoscape:
Network analysis was carried out open source software platform Cytoscape[80] was used. Briefly, genes that were significantly regulated (log2fc ≥ 0.58 or ≤ and adjusted p-value ≤0.05) were curated and subjected to pathway analysis. The graphs were plotted using an in-house R script.

LGEA based analysis for cell types:
The list of genes for major cell types was downloaded from the "LungSortedCells" tool on LGEA database. Here, RNA-seq data defined as belonging to the category "adult" was used as a reference. These data were generated after RNA-sequencing of sorted cells as per the following markers; $CD45^+$ immune cells, $CD45^-/PECAM^-/VECadherin^-/EpCAM^+$ mixed epithelial cells, $CD45^-/PECAM^+/VECadherin^+$ mixed endothelial cells and $CD45^-/PECAM^-/VECadherin^-/EpCAM^-$ mixed mesenchymal cells.
The curation of commonly used lung cell-type markers was done using the LGEA Tool-Box feature. Here, LungGENS Human RNA seq data classified under "Human-Dropseq-PND1" was used as reference.

Second Harmonic generation imaging and sample preparation:
On the day of harvest, the media supernatant was aspirated from each well containing hPCLS. hPCLS were washed with PBS (3X 1ml) and fixed in 1 ml of 4% PFA (EMS EM grade#5710) overnight at 4ºC. Subsequently, hPCLS were washed with PBS (3X). Next, each PFA fixed hPCLS was transferred to a 24 well plate with glass bottom (Greiner senso#662892). hPCLS were covered with 150µl of PBS and pressed to the bottom using a circular glass cover slip and plastic ring (made locally at EMBL workshop). Next, each well was further covered with 300µl of PBS to avoid drying of hPCLS (due to evaporation of PBS in the process of image acquisition).
For live imaging experiment, space between walls of the well and hPCLS was filled with thin layer of 5% low melting agarose to prevent movement due media changes over time in *ex vivo* culture.

SHG imaging of hPCLS was performed on Zeiss NLO LSM780 microscope equipped with a pulsed multiphoton laser. hPCLS were excited with 2-photon wavelength of 880nm with a 20X (0.8 NA, air objective) and a 25X (0.8 NA, water objective) for imaging PFA fixed and live hPCLS respectively. 150-180µm deep z-stacks were acquired with a square tiled (7-8 x 7-8mm) scan. 2-photon excited signals originating from hPCLS were captured in 3 different channels backward SHG, forward SHG and 2-photon excited autofluorescence (2PEA). Forward SHG signal was captured using a laser blocking filter and a band pass filter 436/20 nm. The backward SHG signal was recorded using internal detectors in band width of 435-455 nm. 2PEA was detected in a bandwidth of 550-650 nm.

Calcein-EtHD1 imaging and ATP glo assay:
LIVE/DEAD viability/ cytotoxicity Kit #L3224 (ThermoFisher) was used. Here, on the day of imaging, live hPCLS were washed with 1X phenol free DMEM first and then incubated (45 minutes to 1 hr) with 500µl of 1µM and 2µM working solution of calcein AM and Ethidium homodimer-1 respectively (at 37ºC, 5% CO2). Stained, live hPCLS were transferred into a 35mm mat-tek dish with a glass coverslip in the center (#D35-10-1.5-N). The hPCLS were generally imaged for 20 to 25 minutes in a moist mat-tek chamber with 100µl of phenol free DMEM (Sigma#D2902) covering the hPCLS. After the imaging, hPCLS were discarded. For subsequent day of imaging, new hPCLS were stained and imaged. Cell Titer-Glo Luminescent assay (#G7570, Promega) was used to measure ATP levels. Provider's protocol was used to conduct the assay. Briefly, 1 hPCLS was homogenised using a bead ruptor in 250µl of the CellTiter-Glo Reagent and each hPCLS lysate was measured as triplicates in 96 well plate (50µl triplicates of each hPCLS lysate). And 4 hPCLS were analysed per donor.

Statistical analysis of ELISA and SHG imaging data:
In general, all the data were normalised to the mean value of all the hPCLS measurements (per donor) in the respective control (defined as per the experiment). First, the raw values of SHGintensity(iSHG) from different stimulation or disease conditions were log2 transformed (Log2iSHG), mean iSHG of unstimulated hPCLS was calculated and Log2 transformed (Log2iSHGc). Next Log fold change was calculated as Log2SHGi = Log2iSHG- Log2iSHGc for each slice of the respective donor. Upon global normalization, the Log2iSHG of each hPCLS was normalised to Log2iSHGc of all unstimulated hPCLS across the respective stimulation or condition. Two-way ANOVA with Turkey's multiple comparisons test was performed to obtain significance of the differences between different comparison. Two factors selected were a) differences in donor to donor number of slices b) respective treatment or disease condition. Shapiro-Wilk normality test was used to confirmed data normality.

SHG image analysis:
Image analysis of z-stacks consisting of SHG channels (backward and forward) and 2PEA were analysed using a semi-automated FIJI[81] pipeline defined as Jython script. This pipeline is available as supplementary document as well and is free for usage. Briefly, all the channels were thresholded, the area or the number of pixels under the threshold were counted for each channels (PBT), integrated intensity of PBT was also calculated for each channel (Sumintensity). To measure the total fibrillar collagen content, Sumintensity of PBT of backward and forward SHG signal were summed up and termed as total fibrillar collagen content. A sum of max projections of forward and backward SHG (2D) images was created and this image

was divided into 8x8 equally sized ROIs. Each ROI was manually classified as interstitial collagen or Non-interstitial collagen. Only ROIs of interstitial collagen were averaged per hPCLS SHG image. Each experiment has unstimulated & treated hPCLS SHG images. Sumintensity of total collagen content pixels/ ROI was normalised to the average SHG signal in unstimulated (average of all the ROIs) hPCLS of the respective donor. For each hPCLS SHG stack a minimum of 20 ROIs were analysed.

FIJI code for interstitial and nor-interstitial ROI selection:
Step by step documentation of the code and the code itself is available as a compressed zip file (ImageAnalysis).

Supplementary table legends:
TableS1:
The excel sheet contains the list of all the proteins, their Log2FC with respect to day 1 and corresponding fdr values. These data are from mass spec analysis of unstimulated hPCLS over time (day 1, 4, 7, 10 and 13) in ex vivo culture.
TableS1a:
The excel sheet contains the list of all the proteins that were significantly regulated on day 13 compared to day 1, their Log2FC with respect to day 1 on different days (4, 7, 10 and 13) and corresponding fdr values. These data are from mass spec analysis of unstimulated hPCLS over time (day 1, 4, 7, 10 and 13) in ex vivo culture.
TableS1b:
The excel sheet contains the list of all the Collagens and MMPs were detected from day 1, 4, 7, 10 and 13, their Log2FC with respect to day 1 on different days (4, 7, 10 and 13) and corresponding fdr values. These data are from mass spec analysis of unstimulated hPCLS over time (day 1, 4, 7, 10 and 13) in ex vivo culture.
Table S2:
List of all the metabolites detected over time in unstimulated hPCLS. The list contains Log2FC with respect to day 1 on different days (4, 7, 10 and 13) and corresponding fdr values. These data are from the metabolomic analysis of the hPCLS.
TableS2a:
List of all the annotated metabolites detected over time in unstimulated hPCLS. The list contains Log2FC with respect to day 1 on different days (4, 7, 10 and 13) and corresponding fdr values. These data are from the metabolomic analysis of the hPCLS.
Table S3:
List of all the cell-type specific proteins detected, their Log2FC with respect to day 1 and corresponding fdr values. These data are from mass spec analysis of unstimulated hPCLS over time (day 1, 4, 7, 10 and 13) in ex vivo culture that were compared to LGEA database.
Table S3a:
List of all the cell-type specific proteins detected, that were significantly regulated on day 13 compared to day 1, their Log2FC with respect to day 1 and corresponding fdr values. These data are from mass spec analysis of unstimulated hPCLS over time (day 1, 4, 7, 10 and 13) in ex vivo culture that were compared to LGEA database.

Table S4:
The excel sheet contains the list of all the proteins that were detected on day 13 in Vehicle and TGFß1 treated hPCLS. Their Log2FC with respect to vehicle-treated day 13 hPCLS. These data are from mass spec analysis of vehicle and TGFß1 treated hPCLS (day 13) in ex vivo culture

Table S4a:
The excel sheet contains the list of all the proteins that were significantly regulated in TGFß1 treated hPCLS compared to vehicle-treated hPCLS. These data are from mass spec analysis of vehicle and TGFß1 treated hPCLS (day 13) in ex vivo culture.

Table S5:
List of all the cell-type specific proteins detected, their Log2FC with respect to vehicle-treated hPCLS (day 13) and corresponding fdr values. These data are from mass spec analysis of vehicle and TGFß1 treated hPCLS (day 13) in ex vivo culture and were compared to LGEA database.

Table S6:
These data are from time-course mass spec analysis. Here all the proteins detected are listed. The list is broken into values of each donor and replicate. E.g. Day04_F-S-LT21_rep1, it means changes on day 4 with respect day 1, in a F=Female donor, that has S= active smoker status, is known as with Id= LT21 belongs to replicate. These values are NOT Log2 transformed, hence a value of 1 means no change, below 1 means a decrease and above 1 mean increase with respect to day 1 unstimulated hPCLS.

Table S7:
These data are from vehicle and TGFß1 treated hPCLS (day 13) mass spec analysis. Here all the proteins detected are listed (NA means not detected in that donor or replicate). The list is broken into values of each donor and replicate. E.g. Day04_F-S-LT21_rep1, it means changes on day 4 with respect day 1, in a F=Female donor, that has S= active smoker status, is known as with Id= LT21 belongs to replicate. These values are NOT Log2 transformed, hence a value of 1 means no change, below 1 means a decrease and above 1 mean increase with respect to day 13 vehicle-treated hPCLS.

Table S8:
The table contains raw values of ELISA measurements of each hPCLS per donor.

Table S9:
The table contains raw values of ELISA measurements of each hPCLS per donor upon vehicle or TGFß1 stimulation.

Table S10:
The table contains raw values of ELISA measurements of each hPCLS per donor upon vehicle, TGFß1, MMPi and TGFß1+MMPi stimulation.

Reference:

1. Sakai, N. & Tager, A. M. Fibrosis of two: Epithelial cell-fibroblast interactions in pulmonary fibrosis. *Biochim. Biophys. Acta - Mol. Basis Dis.* **1832**, 911–921 (2013).
2. Wynn, T. A. Common and unique mechanisms regulate fibrosis in various fibroproliferative diseases. *J. Clin. Invest.* **117**, 524–529 (2007).

3. Wynn, T. A. Cellular and molecular mechanisms of fibrosis. *J. Pathol.* **214**, 199–210 (2008).
4. Chapman, H. A. Epithelial-Mesenchymal Interactions in Pulmonary Fibrosis. *Annu. Rev. Physiol.* **73**, 413–435 (2011).
5. Pardo, A. & Selman, M. Matrix metalloproteases in aberrant fibrotic tissue remodeling. *Proc. Am. Thorac. Soc.* **3**, 383–8 (2006).
6. Herrera, J. *et al.* Registration of the extracellular matrix components constituting the fibroblastic focus in idiopathic pulmonary fibrosis. *JCI Insight* **4**, (2019).
7. Karsdal, M. A. *et al.* The good and the bad collagens of fibrosis – Their role in signaling and organ function. *Adv. Drug Deliv. Rev.* **121**, 43–56 (2017).
8. Nanthakumar, C. B. *et al.* Dissecting fibrosis: therapeutic insights from the small-molecule toolbox. *Nat. Rev. Drug Discov.* **14**, 693–720 (2015).
9. Fregonese, L. & Eichler, I. The future of the development of medicines in idiopathic pulmonary fibrosis. *BMC Med.* **13**, 239 (2015).
10. Roach, K. M. *et al.* A model of human lung fibrogenesis for the assessment of anti-fibrotic strategies in idiopathic pulmonary fibrosis. *Sci. Rep.* 1–15 (2018). doi:10.1038/s41598-017-18555-9
11. Hancock, L. A. *et al.* Muc5b overexpression causes mucociliary dysfunction and enhances lung fibrosis in mice. *Nat. Commun.* **9**, 5363 (2018).
12. Tashiro, J. *et al.* Exploring animal models that resemble idiopathic pulmonary fibrosis. *Frontiers in Medicine* **4**, 118 (2017).
13. Sleijfer, S. Bleomycin-Induced Pneumonitis. *Chest* **120**, 617–624 (2001).
14. Selman, M. From Anti-inflammatory Drugs Through Antifibrotic Agents to Lung Transplantation: A Long Road of Research, Clinical Attempts, and Failures in the Treatment of Idiopathic Pulmonary Fibrosis. *Chest* **122**, 759–761 (2002).
15. Raghu G, Anstrom KJ, King TE Jr, Lasky JA, M. F. Prednisone, Azathioprine, and N -Acetylcysteine for Pulmonary Fibrosis. *N. Engl. J. Med.* **366**, 1968–1977 (2012).
16. Stefaniak, M. S., Gandolfi, A. J., Brendel, K., Pretlow, T. P. & Krumdieck, C. L. Agar-filled rat lung slices for use in toxicologic evaluations. (1990).
17. Fisher, R. L. *et al.* The Use of Human Lung Slices in Toxicology. *Hum. Exp. Toxicol.* **13**, 466–471 (1994).
18. Alsafadi, H. N. *et al.* An ex vivo model to induce early fibrosis-like changes in human precision-cut lung slices. *Am. J. Physiol. - Lung Cell. Mol. Physiol.* **312**, L896–L902 (2017).

19. Lehmann, M. *et al.* Differential effects of Nintedanib and Pirfenidone on lung alveolar epithelial cell function in ex vivo murine and human lung tissue cultures of pulmonary fibrosis. 1–12 (2018).
20. Akram, K. M. *et al.* Live imaging of alveologenesis in precision-cut lung slices reveals dynamic epithelial cell behaviour. *Nat. Commun.* **10**, 1178 (2019).
21. Organ, L. A. *et al.* Biomarkers of collagen synthesis predict progression in the PROFILE idiopathic pulmonary fibrosis cohort. *Respir. Res.* **20**, 148 (2019).
22. Cox, G. *et al.* 3-Dimensional imaging of collagen using second harmonic generation. *J. Struct. Biol.* **141**, 53–62 (2003).
23. Mi, H., Muruganujan, A., Ebert, D., Huang, X. & Thomas, P. D. PANTHER version 14: more genomes, a new PANTHER GO-slim and improvements in enrichment analysis tools. *Nucleic Acids Res.* **47**, D419–D426 (2019).
24. Du, Y., Guo, M., Whitsett, J. A. & Xu, Y. 'LungGENS': a web-based tool for mapping single-cell gene expression in the developing lung: Figure 1. *Thorax* **70**, 1092–1094 (2015).
25. Du, Y. *et al.* Lung Gene Expression Analysis (LGEA): an integrative web portal for comprehensive gene expression data analysis in lung development. *Thorax* **72**, 481–484 (2017).
26. Benjamin, M. M. & Khalil, R. A. Matrix metalloproteinase inhibitors as investigative tools in the pathogenesis and management of vascular disease. *Exp. Suppl.* **103**, 209–79 (2012).
27. Brew, K. & Nagase, H. The tissue inhibitors of metalloproteinases (TIMPs): an ancient family with structural and functional diversity. *Biochim. Biophys. Acta* **1803**, 55–71 (2010).
28. Lu, K. V., Jong, K. A., Rajasekaran, A. K., Cloughesy, T. F. & Mischel, P. S. Upregulation of tissue inhibitor of metalloproteinases (TIMP)-2 promotes matrix metalloproteinase (MMP)-2 activation and cell invasion in a human glioblastoma cell line. *Lab. Investig.* **84**, 8–20 (2004).
29. Wang, Z., Juttermann, R. & Soloway, P. D. TIMP-2 Is Required for Efficient Activation of proMMP-2 in Vivo. *J Biol Chem.* **275**, 26411–26415 (2009).
30. Chelladurai, P., Seeger, W. & Pullamsetti, S. S. Series 'matrix metalloproteinases in lung health and disease': Matrix metalloproteinases and their inhibitors in pulmonary hypertension. *Eur. Respir. J.* **40**, 766–782 (2012).
31. Fuhrer, T., Heer, D., Begemann, B. & Zamboni, N. High-Throughput, Accurate Mass Metabolome Profiling of Cellular Extracts by Flow Injection–Time-of-Flight Mass Spectrometry. *Anal.*

Chem. **83**, 7074–7080 (2011).
32. Meng, X., Nikolic-paterson, D. J. & Lan, H. Y. TGF-β: the master regulator of fibrosis. *Nat. Publ. Gr.* (2016). doi:10.1038/nrneph.2016.48
33. Smit, M. *et al.* Bronchoconstriction Induces TGF-β Release and Airway Remodelling in Guinea Pig Lung Slices. *PLoS One* **8**, e65580 (2013).
34. Leeming, D. J. *et al.* Serological investigation of the collagen degradation profile of patients with chronic obstructive pulmonary disease or idiopathic pulmonary fibrosis. *Biomark. Insights* **7**, 119–126 (2012).
35. Leeming, D. J. *et al.* Enzyme-linked immunosorbent serum assays (ELISAs) for rat and human N-terminal pro-peptide of collagen type I (PINP) — Assessment of corresponding epitopes. *Clin. Biochem.* **43**, 1249–1256 (2010).
36. Huang, X. *et al.* Molecular characterization of a precision-cut rat lung slice model for the evaluation of antifibrotic drugs. *Am J Physiol Lung Cell Mol Physiol* **316**, 348–357 (2019).
37. Sweetwyne, M. T. & Murphy-Ullrich, J. E. Thrombospondin1 in tissue repair and fibrosis: TGF-β-dependent and independent mechanisms. *Matrix Biol.* **31**, 178–86 (2012).
38. Reinecke, H. *et al.* Lack of thrombospondin-2 reduces fibrosis and increases vascularity around cardiac cell grafts. *Cardiovasc. Pathol.* **22**, 91–95 (2013).
39. Estany, S. *et al.* Lung fibrotic tenascin-C upregulation is associated with other extracellular matrix proteins and induced by TGFβ1. *BMC Pulm. Med.* **14**, 120 (2014).
40. Staab-Weijnitz, C. A. *et al.* FK506-Binding Protein 10, a Potential Novel Drug Target for Idiopathic Pulmonary Fibrosis. *Am. J. Respir. Crit. Care Med.* **192**, 455–467 (2015).
41. Fernandez, I. E. & Eickelberg, O. The Impact of TGF- b on Lung Fibrosis From Targeting to Biomarkers. doi:10.1513/pats.201203-023AW
42. Awasthi, S. *et al.* Detecting the Molecular System Signatures of Idiopathic Pulmonary Fibrosis through Integrated Genomic Analysis. *Sci. Rep.* **7**, 1–11 (2017).
43. Knudsen, L., Ruppert, C. & Ochs, M. Tissue remodelling in pulmonary fibrosis. *Cell Tissue Res.* **367**, 607–626 (2017).
44. Hardie, W. D. *et al.* Signaling pathways in the epithelial origins of pulmonary fibrosis. *Cell Cycle* **9**, 2769–2776 (2010).
45. O'Dwyer, D. N. *et al.* Erratum: The peripheral blood proteome signature of idiopathic pulmonary fibrosis is distinct from normal and is associated with novel immunological processes. *Sci. Rep.* **7**,

46860 (2017).
46. Cox, G. & Kable, E. Second-harmonic imaging of collagen. *Methods Mol. Biol.* **319**, 15–35 (2006).
47. Liu, W., Raben, N. & Ralston, E. Quantitative evaluation of skeletal muscle defects in second harmonic generation images. *J. Biomed. Opt.* **18**, 026005 (2013).
48. Yu, C.-H. *et al.* Measuring microtubule polarity in spindles with second-harmonic generation. *Biophys. J.* **106**, 1578–87 (2014).
49. Kuhn, C. *et al.* An Immunohistochemical Study of Architectural Remodeling and Connective Tissue Synthesis in Pulmonary Fibrosis. *Am. Rev. Respir. Dis.* **140**, 1693–1703 (1989).
50. Hansen, N. U. B. *et al.* Tissue turnover of collagen type I, III and elastin is elevated in the PCLS model of IPF and can be restored back to vehicle levels using a phosphodiesterase inhibitor. *Respir. Res.* **17**, 1–10 (2016).
51. Han, S., Li, Y. Y. & Chan, B. P. Protease inhibitors enhance extracellular collagen fibril deposition in human mesenchymal stem cells. *Stem Cell Res. Ther.* **6**, 197 (2015).
52. Dancer, R. C. A., Wood, A. M. & Thickett, D. R. Metalloproteinases in idiopathic pulmonary fibrosis. *Eur. Respir. J.* **38**, 1461–7 (2011).
53. Adams, T. S. *et al.* Single-cell RNA-seq reveals ectopic and aberrant lung-resident cell populations in idiopathic pulmonary fibrosis. *Sci. Adv.* **6**, eaba1983 (2020).
54. Habermann, A. C. *et al.* Single-cell RNA sequencing reveals profibrotic roles of distinct epithelial and mesenchymal lineages in pulmonary fibrosis. *Sci. Adv.* **6**, eaba1972 (2020).
55. Travaglini, K. J. *et al.* A molecular cell atlas of the human lung from single-cell RNA sequencing. *Nature* **587**, 619–625 (2020).
56. Zhang, Q. *et al.* Landscape and Dynamics of Single Immune Cells in Hepatocellular Carcinoma. *Cell* **179**, 829-845.e20 (2019).
57. Stegmayr, J. *et al.* Isolation of high yield and quality RNA from human precision-cut lung slices for RNA-sequencing and computational integration with larger patient cohorts. *Am. J. Physiol. Lung Cell. Mol. Physiol.* (2020). doi:10.1152/ajplung.00401.2020
58. Leeming, D. J. *et al.* Enzyme-linked immunosorbent serum assays (ELISAs) for rat and human N-terminal pro-peptide of collagen type I (PINP) — Assessment of corresponding epitopes. *Clin. Biochem.* **43**, 1249–1256 (2010).
59. Gabr, S. A., Alghadir, A. H., Sherif, Y. E. & Ghfar, A. A. Hydroxyproline as a Biomarker in Liver Disease. doi:10.1007/978-94-007-7742-2_26-1
60. Hewitson, T. D., Smith, E. R., Samuel, C. S. & Professor, A. /.

Qualitative and quantitative analysis of fibrosis in the kidney ABSTRACT. (2014). doi:10.1111/nep.12321
61. Puthawala, K. *et al.* Inhibition of Integrin αvβ6, an Activator of Latent Transforming Growth Factor-β, Prevents Radiation-induced Lung Fibrosis. *Am. J. Respir. Crit. Care Med.* **177**, 82–90 (2008).
62. Page-mccaw, A., Ewald, A. J. & Werb, Z. Matrix metalloproteinases and the regulation of tissue remodelling. **8**, 221–233 (2009).
63. Zank, D. C., Bueno, M., Mora, A. L. & Rojas, M. Idiopathic Pulmonary Fibrosis: Aging, Mitochondrial Dysfunction, and Cellular Bioenergetics. *Front. Med.* **5**, 10 (2018).
64. Nicholson, A. G. *et al.* Three-dimensional characterization of fibroblast foci in idiopathic pulmonary fibrosis. *JCI Insight* (2016). doi:10.1172/jci.insight.86375
65. Arora, P. D., Narani, N. & McCulloch, C. A. G. The compliance of collagen gels regulates transforming growth factor-β induction of α-smooth muscle actin in fibroblasts. *Am. J. Pathol.* **154**, 871–882 (1999).
66. Wipff, P.-J., Rifkin, D. B., Meister, J.-J. & Hinz, B. Myofibroblast contraction activates latent TGF-β1 from the extracellular matrix. *J. Cell Biol.* **179**, 1311–1323 (2007).
67. Zscheppang, K. *et al.* Human Pulmonary 3D Models For Translational Research. *Biotechnol. J.* **13**, 1–12 (2018).
68. Desai, O., Winkler, J., Minasyan, M. & Herzog, E. L. The role of immune and inflammatory cells in idiopathic pulmonary fibrosis. *Front. Med.* **5**, (2018).
69. Mercer, P. F. *et al.* Exploration of a potent PI3 kinase/mTOR inhibitor as a novel anti-fibrotic agent in IPF. *Thorax* **71**, 701–11 (2016).
70. Gerckens, M. *et al.* Generation of Human 3D Lung Tissue Cultures (3D-LTCs) for Disease Modeling. *J. Vis. Exp.* 1–8 (2019). doi:10.3791/58437
71. Barascuk, N. *et al.* A novel assay for extracellular matrix remodeling associated with liver fibrosis: An enzyme-linked immunosorbent assay (ELISA) for a MMP-9 proteolytically revealed neo-epitope of type III collagen. *Clin. Biochem.* **43**, 899–904 (2010).
72. Bager, C. L. *et al.* Quantification of fibronectin as a method to assess ex vivo extracellular matrix remodeling. *Biochem. Biophys. Res. Commun.* **478**, 586–591 (2016).
73. Bantscheff, M., Schirle, M., Sweetman, G., Rick, J. & Kuster, B. Quantitative mass spectrometry in proteomics: a critical review. *Anal. Bioanal. Chem.* **389**, 1017–1031 (2007).
74. Werner, T. *et al.* Ion Coalescence of Neutron Encoded TMT 10-

Plex Reporter Ions. *Anal. Chem.* **86**, 3594–3601 (2014).
75. Savitski, M. M. *et al.* Measuring and Managing Ratio Compression for Accurate iTRAQ/TMT Quantification. *J. Proteome Res.* **12**, 3586–3598 (2013).
76. Fuhrer, T., Heer, D., Begemann, B. & Zamboni, N. High-Throughput, Accurate Mass Metabolome Profiling of Cellular Extracts by Flow Injection–Time-of-Flight Mass Spectrometry. *Anal. Chem.* **83**, 7074–7080 (2011).
77. Wishart, D. S. *et al.* HMDB 4.0: the human metabolome database for 2018. *Nucleic Acids Res.* **46**, D608–D617 (2018).
78. Ritchie, M. E. *et al.* limma powers differential expression analyses for RNA-sequencing and microarray studies. *Nucleic Acids Res.* **43**, e47 (2015).
79. Huber, W., von Heydebreck, A., Sültmann, H., Poustka, A. & Vingron, M. Variance stabilization applied to microarray data calibration and to the quantification of differential expression. *Bioinformatics* **18 Suppl 1**, S96-104 (2002).
80. Shannon, P. *et al.* Cytoscape: A Software Environment for Integrated Models of Biomolecular Interaction Networks. *Genome Res.* **13**, 2498–2504 (2003).
81. Schindelin, J. *et al.* Fiji: an open-source platform for biological-image analysis. *Nat. Methods* **9**, 676–682 (2012).

General description

Jython script for Fiji for processing and quantifying collagen deposition on the microscopy images of high precision cut lung slices (hPCLS).

Contributors

- Muzamil Majid Khan (Pepperkok Lab): project runner, main user and tester
- Christian Tischer (CBA): initial development
- Aliaksandr Halavatyi (ALMF): development and support

Dependencies:

- Fiji
- AutoMicTools library

See Documentation for the guidelines

Documentation

Under this link you will find the detailed description of the tool functions and step-by-step guidelines for its use.

Citation

Please cite following work when using this tool:

> Multiomic and quantitative label-free microscopy-based analysis of ex vivo culture and TGFbeta1 stimulation of human precision-cut lung slices
> Muzamil Majid Khan, Daniel Poeckel, Aliaksandr Halavatyi, Frank Stein, Johanna Vappiani, Daniel C. Sevin, Christian Tischer, Nico Zinn, Jess D Eley, Natasja Stæhr Gudmann, Thomas Muley, Hauke Winter, Andrew J Fisher, Carmel B. Nanthakumar, Giovanna Bergamini, Rainer Pepperkok
> bioRxiv 2019.12.13.875963; doi: https://doi.org/10.1101/2019.12.13.875963

Contact

Please contact Muzamil Majid Khan (muzamil.m.khan@embl.de) and Aliaksandr Halavatyi (aliaksandr.halavatyi@embl.de) if you have questions, comments or suggestions about using this tool.

Selective analysis of interstitial collagen in hPCLS

General information

This Jython script is dedicated for processing 3D multichannel images of high precision cut lung slices (hPCLS) in order to quantify collagen deposition. Script performs either fully automated or semi-automated analysis of multiple image datasets:

- For each individual input channel
  - Creates binary masks for z-stacks by applying user-specified thresholds => **BW** images.
  - Applies created masks on the original image stacks and converts background pixles to 0 => **GATED** images
  - Measures the number of object pixels **BW** images (as measure of deposited collagen volume) and sum of intensities of **GATED** images (as measure of the amount of deposited collagen).
- Creates masks for overlaps and combinations of masks of different channels => **PBT** images.
  Quantifies number of positive (object) pixels on these images.
- Creates 2D projection of collagen deposition by summing up max projections of specified channels (e.g. forward and backward harmonic), in which representative images are acquired.
- Creates a grid of regions on the input image and performs all measurements listed above in the individual regions. Optionally, allows user to interactively delete regions from the analysis.
- Saves all produced images
- Saves all quantifications and links to generated image files in a tabular format. Data can be interactively browsed using cabalities of AutoMicTools library (see Browsing of analysis results section below).

Installation

- **Install Fiji** if you did not have installed it before.
- **Install AutomicTools library**. Dowhload `AutoMic_JavaTools-xxx.jar` file from here and copy it to the plugins subdirectory of your Fiji installation. Fiji needs to be restarted afterwards.

> Note: `hPCLS-microscopy-image-analysis.py` was tested with AutoMicTools version 1.1.4 released on January, 3 2019, but it is recommended to use the latest available version of AutoMicTools.

- **Download `hPCLS-microscopy-image-analysis.py` script** to your computer and open it in Fiji either by *Drag-And-Drop* into Fiji status bar or via main dialog (*File->Open*).

Input data format

Folder with image files to be analysed. Input image files have to satisfy the following requirements:

- Images should be compatible with Bio-Formats ImageJ plugin, because the script uses Bio-Formats for image opening.
- Each file has to contain one dataset (images from single stage position).
- Images for Z-slices and channels of one dataset have to be in the same file.
- Time-lapse data can be analysed, but images for different timepoints have to be in different files.
- All image files in the same input folder should have the same format:
  - Bit depth
  - Number of z-slices
  - Number and order of channels
- If tile scans are acquired to cover complete slice area, stitching has to be performed before starting the script.

Output data format

Output folder, containing:

- Text files with result tables
- Subfolders with generated images

Output folder is created automatically under the same path where input folder is located. Name of the output folder has format < *name-of-input-folder* >*--fiji*

> Note: If such folder already exists, script will automatically erase all its content before analysis is started. Rename folder with the results of the previous analysis if you want to keep these data along with the results of new analysis.

Text files contain tab-separated tabular data with references to input and generated images, as well as quantifications. There are two output tables:

- *analysis_summary_image.txt*: ane line corresponds to one dataset (image). Numbers in the numeric columns correspond to the measurements for for the whole z-tack (PCLS).
- *analysis_summary_regions.txt*: One line corresponds to one region in the grid pattern. Numbers are for each ROI/PCLS. This table has all the columns that are present in image table and references to the quantified regions. These references allow visualise quantified regions with the ***AutoMic Browser*** tool after analysis (see Browsing of analysis results section below).

Names of the numeric columns in both files have format:

- ***PBT.x_NUM***: Number of the threshold pixels in channel x
- ***SumIntensity.x_NUM***:Sum intensity of the gated image in channel x
- ***PBT.xANDy_NUM***: Number of pixels common between respective channels
- ***PBT.1OR2OR3_NUM***: Number of pixels positive in either of three channels (multiple pixels positive in different channels only counted once).

Generated images are stored in the appropriate subfolders with the names of the files corresponding to the names of the input images:

- ***BW.x***: Binary masks of channel x.
- ***GATED.x***: Gated stack for channel X
- ***Second.Harmonic.Max.Proj*** folder contains processed image which is a sum of max projections of the channels defined in the analysis parameters

Workflow

Data processing

1. Open the script in FIJI
2. Press **Run** button in the script window to start the analysis
3. Specify analysis parameters:
   - **Datasets to analyse**: either ***all*** (default) or index of the dataset to be analysed (for testing).
   - **Input File Extension**: only image files with specified extension will be analysed.
   - **Number of Channels**: only images with specified number of channels will be analysed.
   - **Input Data Path**: path to the input folder with images to process.
   - **Filter grid regions manually**: select this option for interactive selection of the grid regions which have to be excluded from the analysis
   - **Region Split X** and **Region split Y**: the dimensions of ROIs grid that the images are divided into for the region analysis (e.g. 3X3 or more).
4. Press **OK** to continue
5. Specify channel-specific parameters in the second dialog:
   - The threshold values for signal in each channel (the values can be estimated before running the script manually or via the test run of the script)
   - **Sum of Channels for Segmentation**: the indexes of the channels for which max need to be combined for defining analysis regions.
6. Press **OK** to start the analysis. Follow the analysis progress in the console panel of the script window. At the same time AutoMic Browser tool will open automatically with the image-based table. Measured values will appear in the table during the analysis.
7. If **Filter grid regions manually** option was selected, projected images will pop up automatically superexposed by the defined number of ROIs.
   Delete the ROIS that are not required from the ROI manager (removed regions will not appear in the region-based table).
   For selecting discarded regions directly from the image use the following steps (more info here)
   - "Hand" tool in Fiji has to be activated (grid script activates in automatically).
   - **Ctrl+ mouse click** (**Cmd + mouse click** for Mac) on the image selects corresponding ROI in RoiManager. Pressing **Del** will remove corresponding ROI from RoiManager (multiple regions can not be selected this way).
   - If region selected by mistake, another region can not be selected. Can press **Ctrl++Shift+A** to deselect all regions, then new selection is possible.
8. When the analysis is completed, the *Analysis finished* message will appear in the console panel.

Browsing of analysis results

Generated text files can be opened in either spreadsheet software (e.g. MS Excel) or statistical packages (e.g. R) and subjected to analysis as per the user's needs.

Alternatively, these tables can be browsed with the special Fiji plugin ***AutoMic Browser***, which allows easily navigate through the datasets and correlate measurements to corresponding images and ROIs:

- *AutoMicTools* package in Fiji needs to be installed (see Installation).
- Start ***AutoMic Browser***: *Plugins->Auto Mic Tools -> AutoMic Browser*
- Select one of generated test files in the dialog.
- Specify which images have to be visualised by ticking appropriate checkboxes in the bottom panel.
- Recommended optional visualisation parameters (bottom left panel):
  - Select **Fit image to the frame** to appropriately scale big images into corresponding windows
  - Select ***Min_max*** option in the **Image Contrast** drop box to adjust contrast automatically when another image is opened.
- Tick **Region.Roi** checkboxes under appropriate image headers to outline region that corresponds to the selected dataset (only for region-based table).
- Click on different lines of the table to navigate through the datasets. Content of image windows will be updated accordingly.

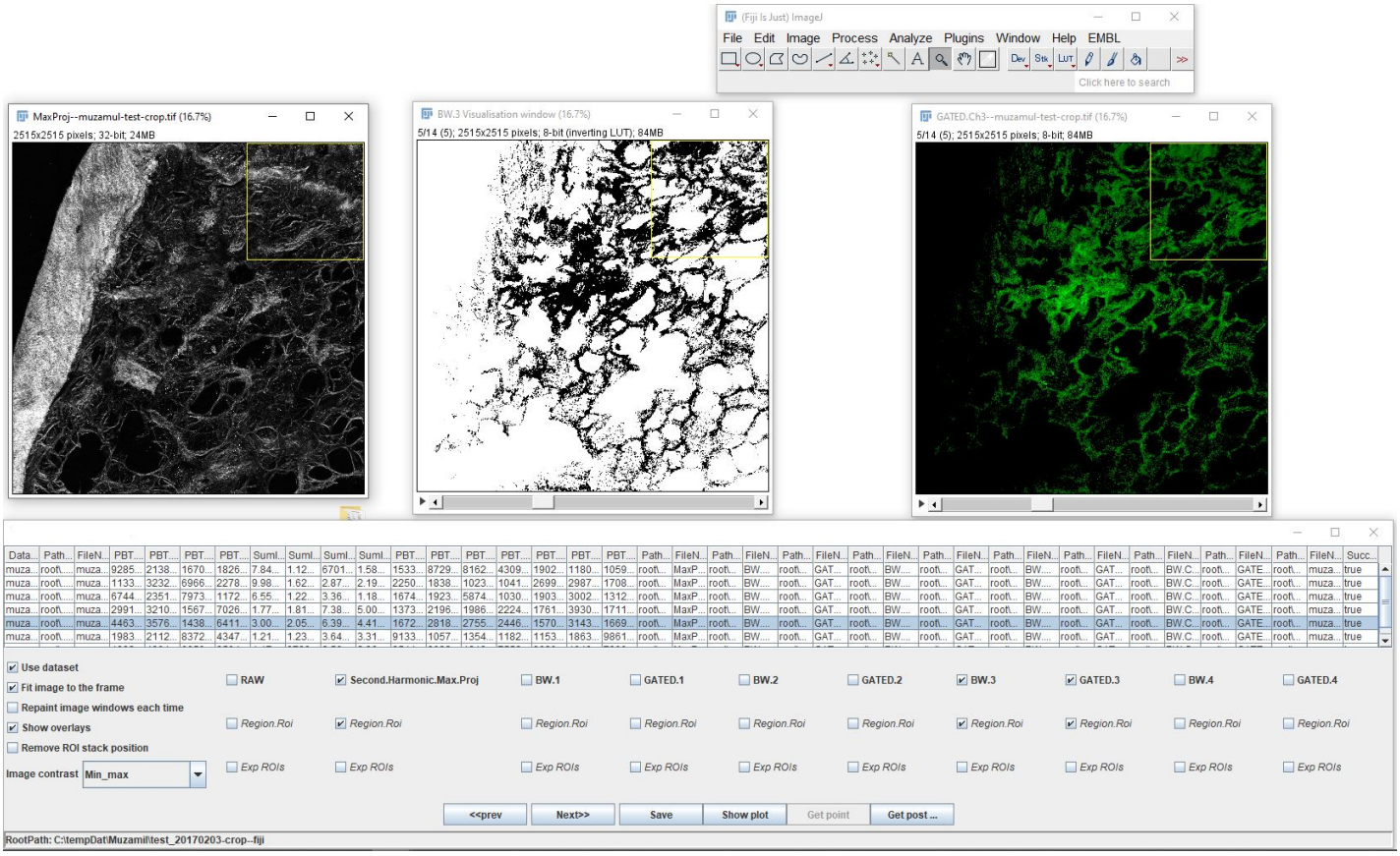

The **AutoMic Browser** tool can be used to quality control analysis results:

- In the table panel select line with the measurements that have have to be excluded from the downstream analysis.
- Unselect **Use dataset** checkbox. Corresponding value in the last column of the table(*Success_BOOL*) will changle from ***true*** to ***false***.
- Press **Save** button to save modified table (new table is always save in the same folder as the original table, therefore only file name needs to be specified).

Figure 1

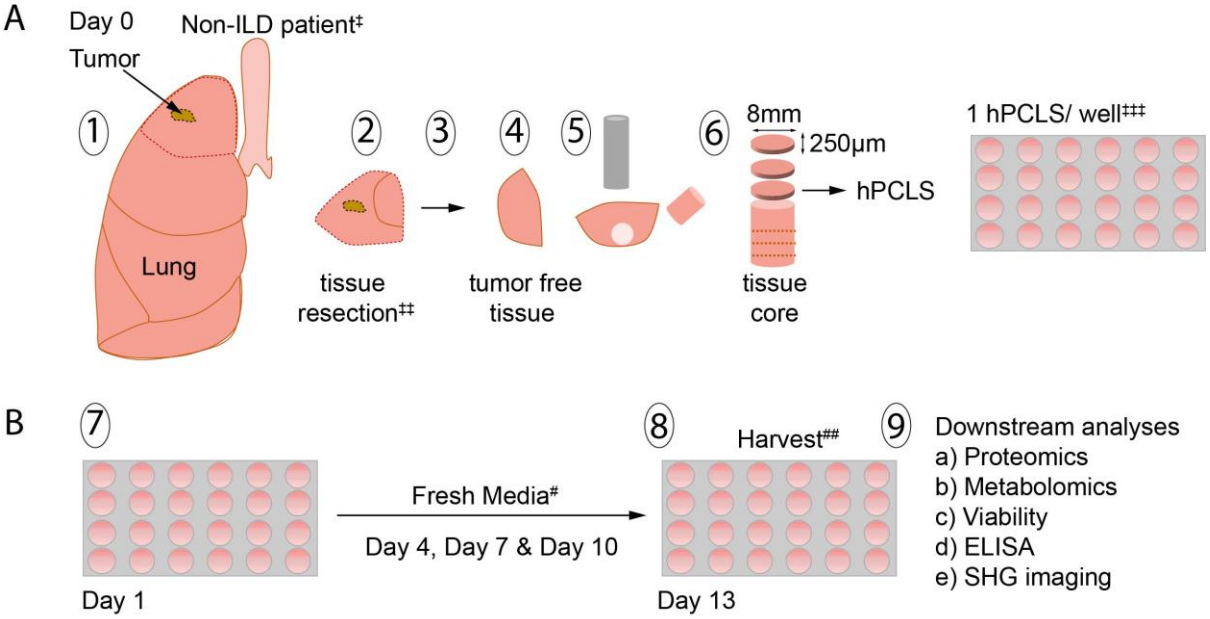
A
Day 0
Non-ILD patient‡
Tumor
Lung
1
2
3
4
5
6
tissue resection‡‡
tumor free tissue
8mm
250µm
hPCLS
tissue core
1 hPCLS/ well‡‡‡
B
7
8
Harvest###
9
Fresh Media#
Day 4, Day 7 & Day 10
Day 1
Day 13
Downstream analyses
a) Proteomics
b) Metabolomics
c) Viability
d) ELISA
e) SHG imaging

Figure 2

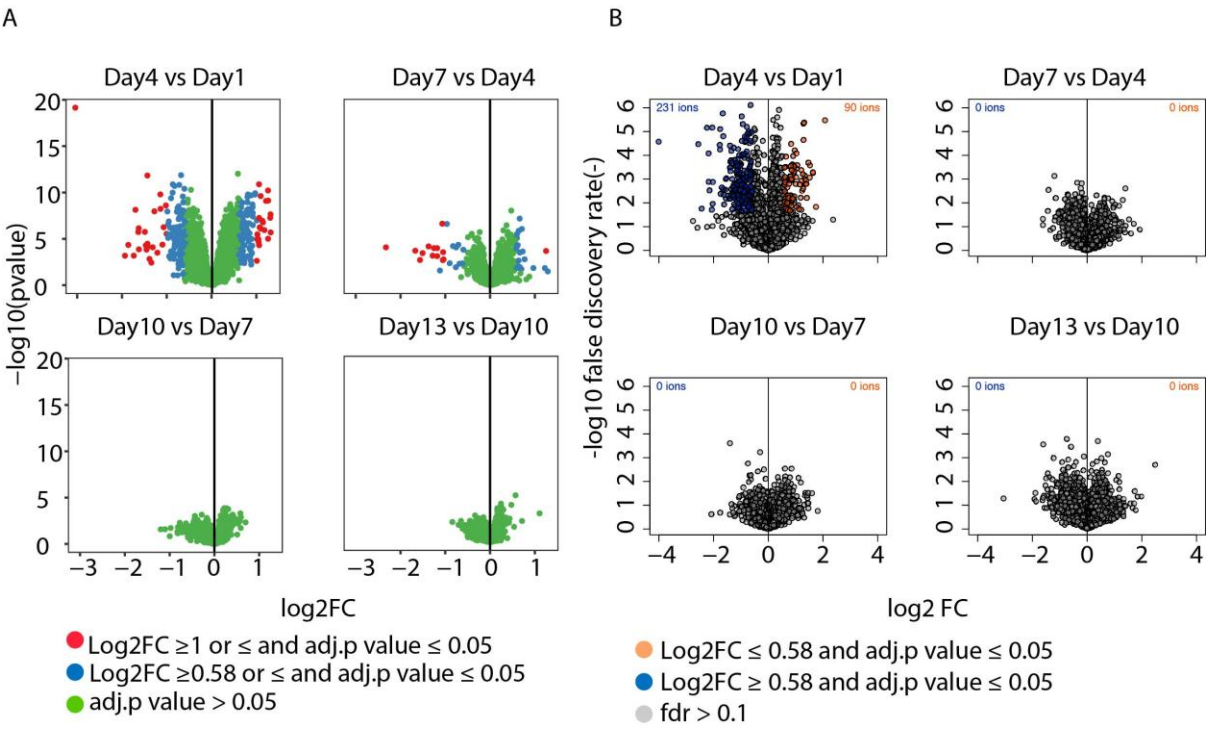
A
Day4 vs Day1
Day7 vs Day4
Day10 vs Day7
Day13 vs Day10
−log10(pvalue)
log2FC
Log2FC ≥1 or ≤ and adj.p value ≤ 0.05
Log2FC ≥0.58 or ≤ and adj.p value ≤ 0.05
adj.p value > 0.05
B
Day4 vs Day1
Day7 vs Day4
Day10 vs Day7
Day13 vs Day10
231 ions
90 ions
0 ions
0 ions
-log10 false discovery rate(-)
log2 FC
Log2FC ≤ 0.58 and adj.p value ≤ 0.05
Log2FC ≥ 0.58 and adj.p value ≤ 0.05
fdr > 0.1

Figure 3

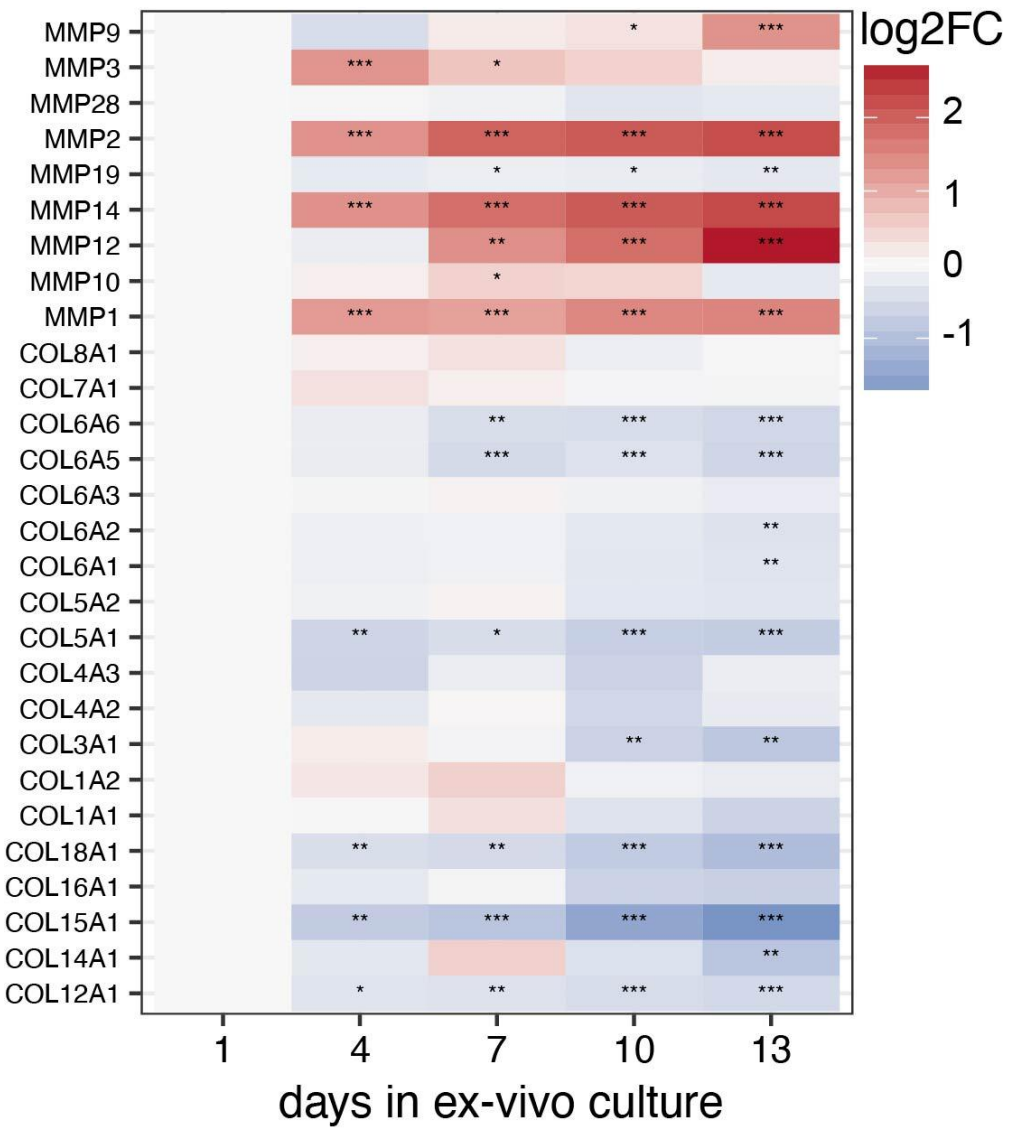
MMP9
MMP3
MMP28
MMP2
MMP19
MMP14
MMP12
MMP10
MMP1
COL8A1
COL7A1
COL6A6
COL6A5
COL6A3
COL6A2
COL6A1
COL5A2
COL5A1
COL4A3
COL4A2
COL3A1
COL1A2
COL1A1
COL18A1
COL16A1
COL15A1
COL14A1
COL12A1
1
4
7
10
13
days in ex-vivo culture
log2FC
2
1
0
-1

Figure 4

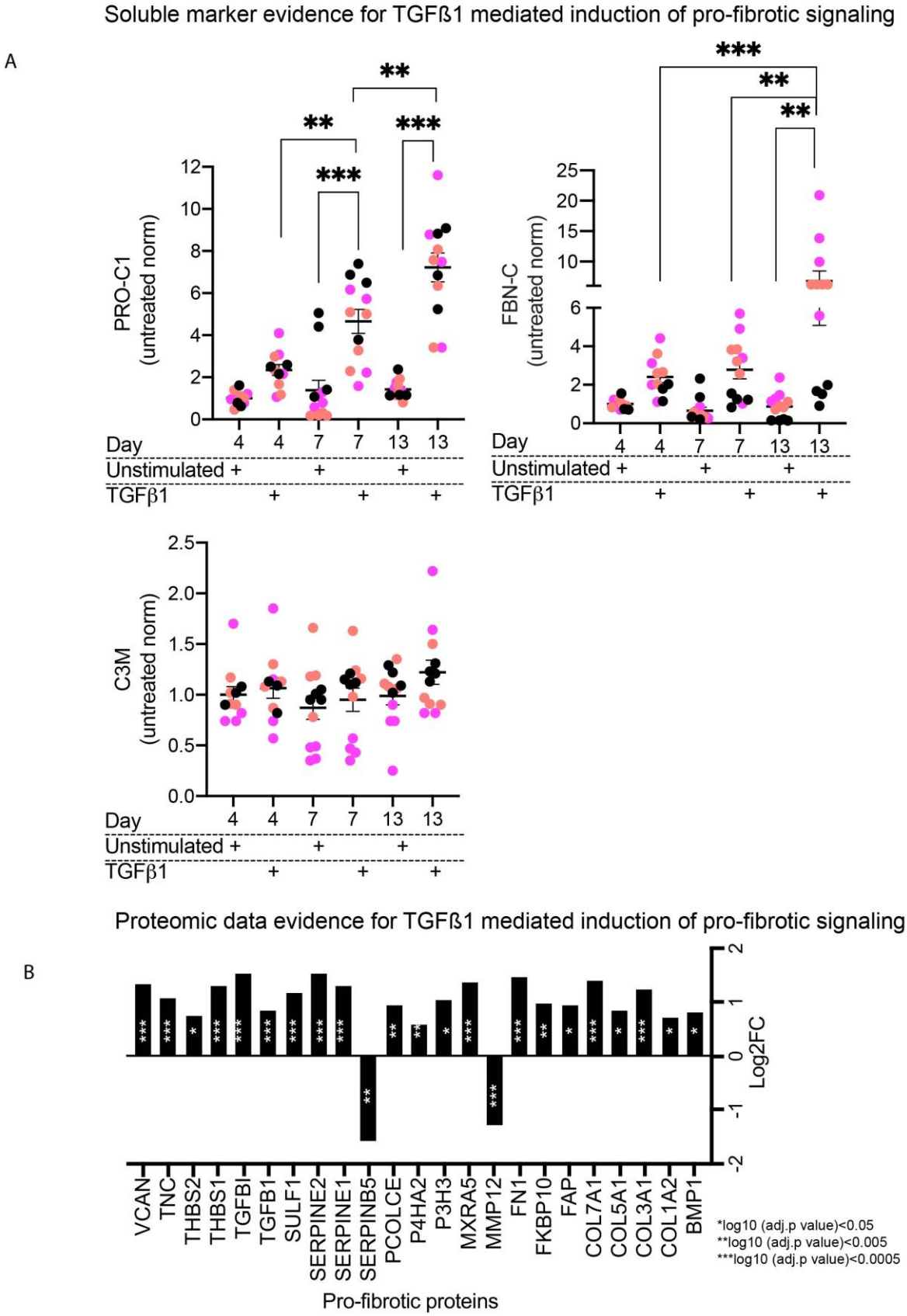
Soluble marker evidence for TGFß1 mediated induction of pro-fibrotic signaling
A
PRO-C1 (untreated norm)
FBN-C (untreated norm)
C3M (untreated norm)
Day
Unstimulated
TGFβ1
Proteomic data evidence for TGFß1 mediated induction of pro-fibrotic signaling
B
Log2FC
VCAN
TNC
THBS2
THBS1
TGFBI
TGFB1
SULF1
SERPINE2
SERPINE1
SERPINB5
PCOLCE
P4HA2
P3H3
MXRA5
MMP12
FN1
FKBP10
FAP
COL7A1
COL5A1
COL3A1
COL1A2
BMP1
Pro-fibrotic proteins
*log10 (adj.p value)<0.05
**log10 (adj.p value)<0.005
***log10 (adj.p value)<0.0005

!

Figure 5

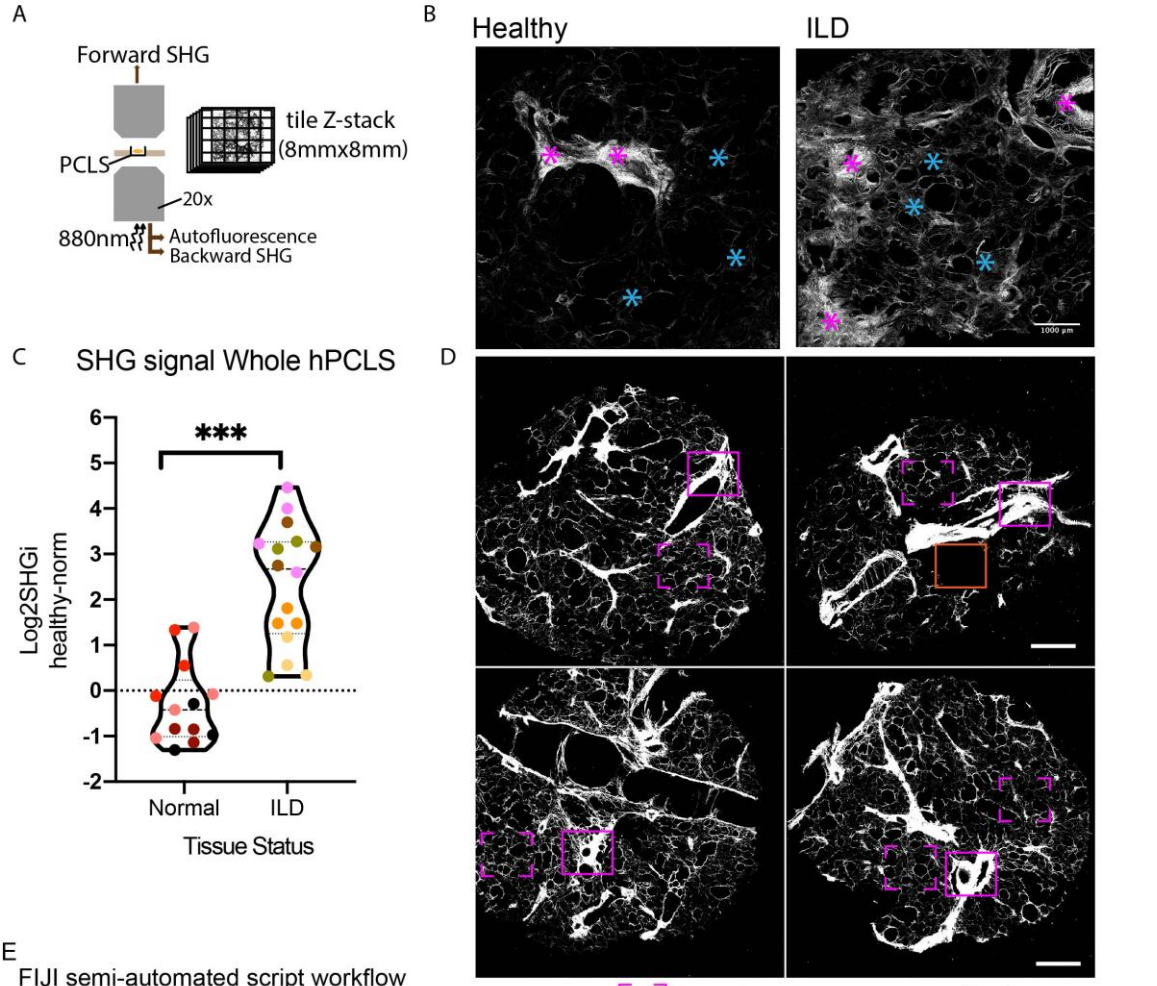

E

FIJI semi-automated script workflow

a) Threshold

b) Division into ROI tiles 8x8

c) Only 3D ROIs of Alveoli and interstitium quantified (manual selection)

d) 3D Integrated density(i)/ROI

e) Total fibrillar collagen = $FSHG_{intensity}$+$BSHG_{intensity}$

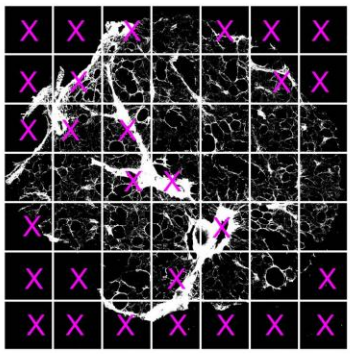

Interstitial fibrillar collagen SHG signal

Airway/ blood vessel fibrillar collagen SHG signal

hPCLS preparation induced damage/ artifact

F

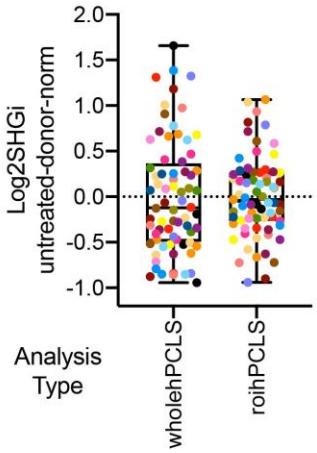

Figure 6

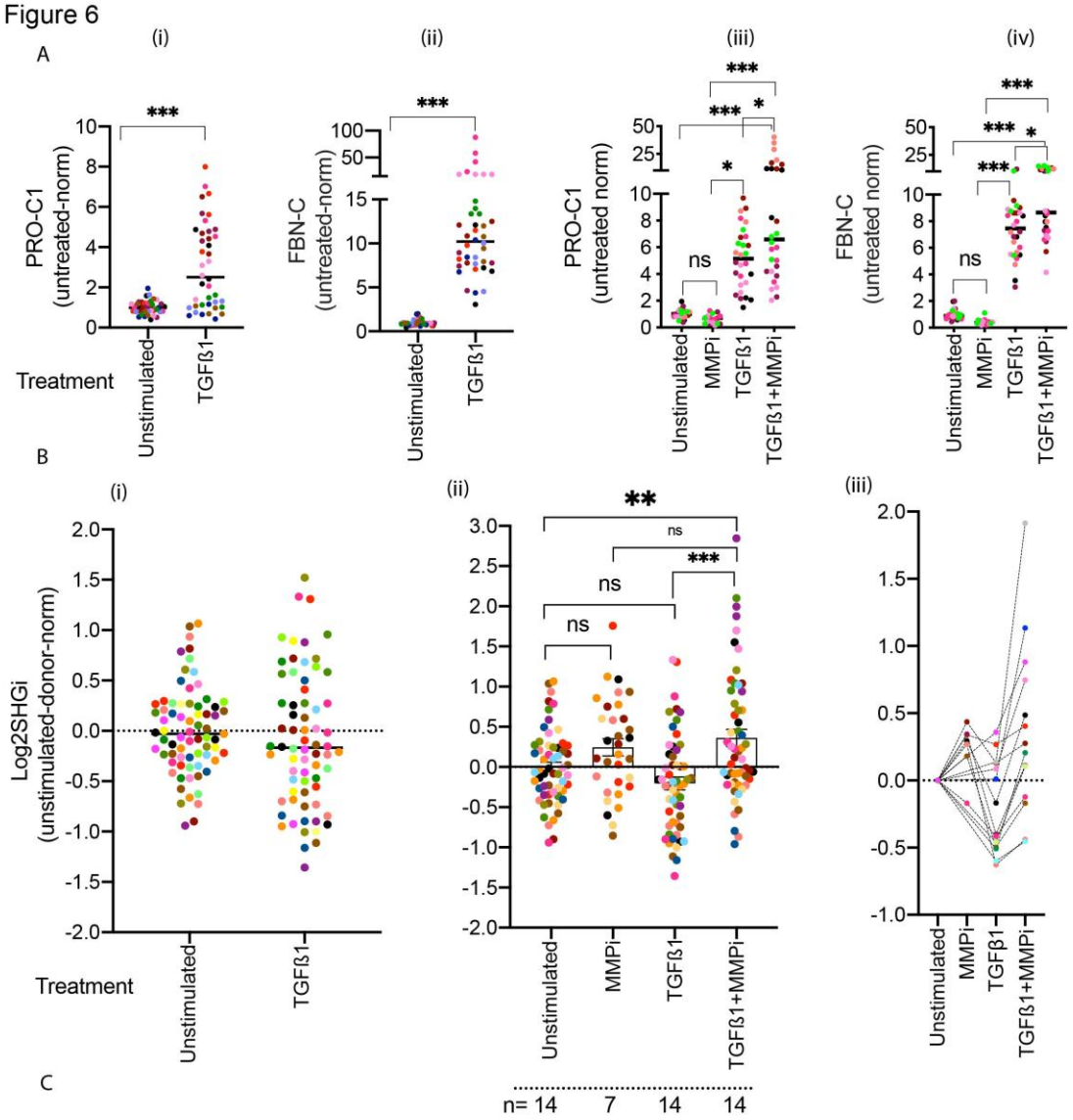
A
(i)
(ii)
(iii)
(iv)
PRO-C1 (untreated-norm)
FBN-C (untreated-norm)
PRO-C1 (untreated norm)
FBN-C (untreated norm)
***
*
ns
Unstimulated
MMPi
TGFß1
TGFß1+MMPi
Treatment
B
(i)
(ii)
(iii)
Log2SHGi (unstimulated-donor-norm)
**
ns
n= 14 7 14 14

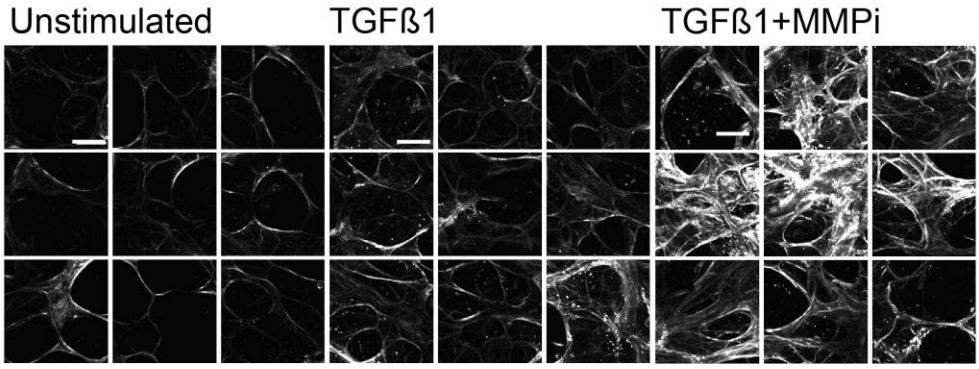
C
Unstimulated
TGFß1
TGFß1+MMPi

Figure S2

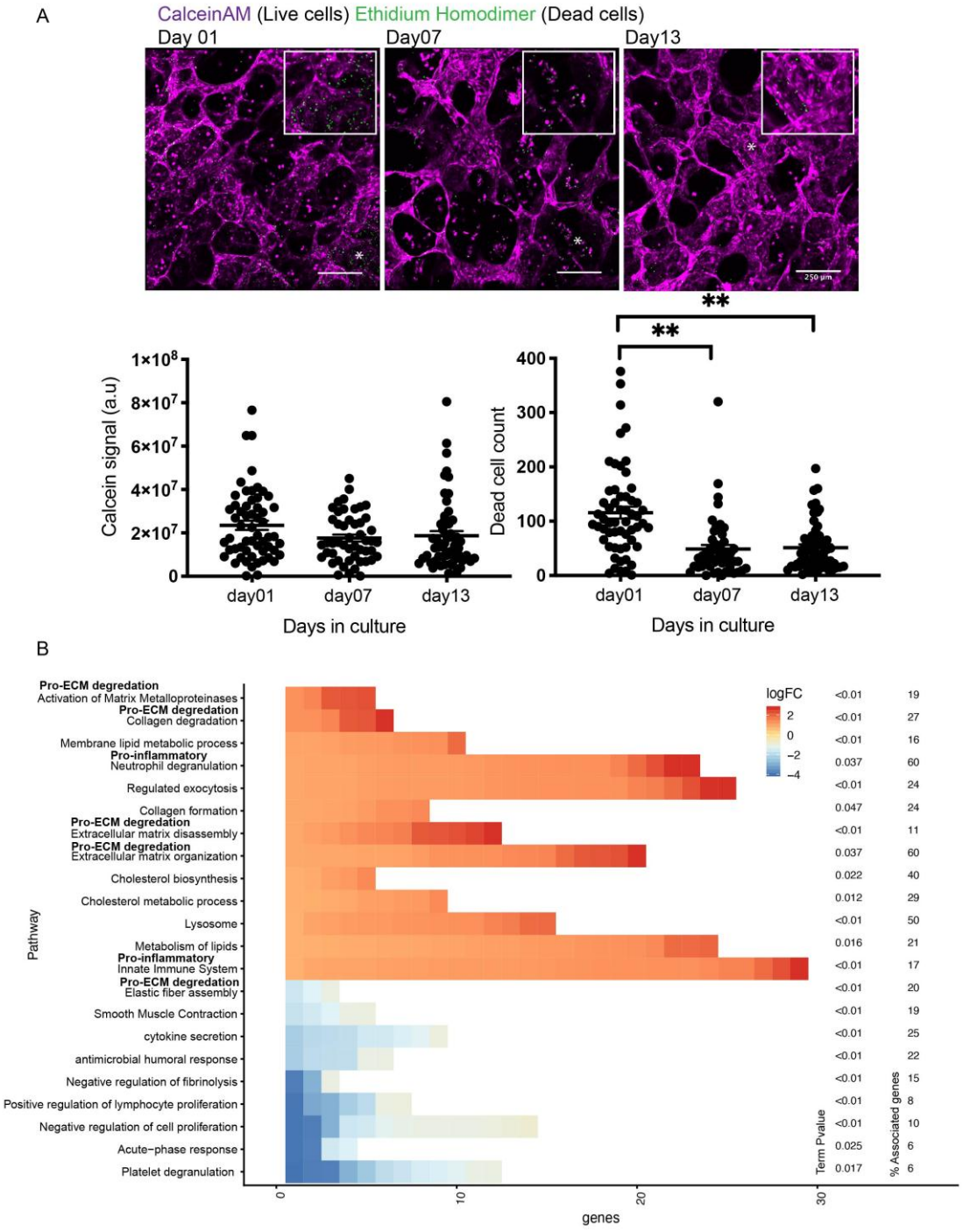
A
CalceinAM (Live cells) Ethidium Homodimer (Dead cells)
Day 01
Day07
Day13
250 µm
Calcein signal (a.u)
1×10^8
8×10^7
6×10^7
4×10^7
2×10^7
0
day01
day07
day13
Days in culture
Dead cell count
400
300
200
100
0
**
**
day01
day07
day13
Days in culture
B
Pro-ECM degredation
Activation of Matrix Metalloproteinases
Pro-ECM degredation
Collagen degradation
Membrane lipid metabolic process
Pro-inflammatory
Neutrophil degranulation
Regulated exocytosis
Collagen formation
Pro-ECM degredation
Extracellular matrix disassembly
Pro-ECM degredation
Extracellular matrix organization
Cholesterol biosynthesis
Cholesterol metabolic process
Lysosome
Metabolism of lipids
Pro-inflammatory
Innate Immune System
Pro-ECM degredation
Elastic fiber assembly
Smooth Muscle Contraction
cytokine secretion
antimicrobial humoral response
Negative regulation of fibrinolysis
Positive regulation of lymphocyte proliferation
Negative regulation of cell proliferation
Acute−phase response
Platelet degranulation
Pathway
logFC
2
0
−2
−4
<0.01 19
<0.01 27
<0.01 16
0.037 60
<0.01 24
0.047 24
<0.01 11
0.037 60
0.022 40
0.012 29
<0.01 50
0.016 21
<0.01 17
<0.01 20
<0.01 19
<0.01 25
<0.01 22
<0.01 15
<0.01 8
<0.01 10
0.025 6
0.017 6
Term Pvalue
% Associated genes
0
10
20
30
genes

Figure S2 C

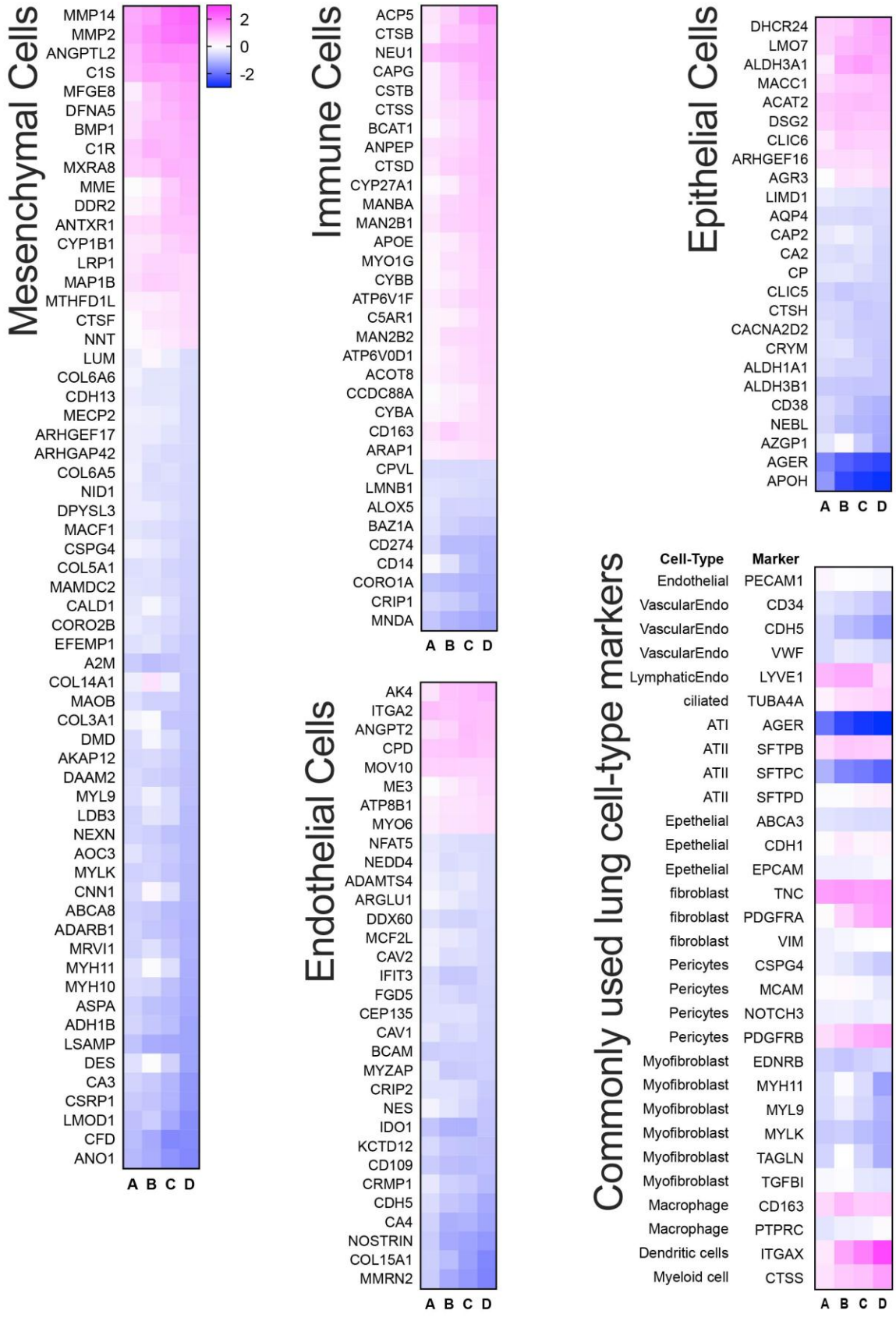
Mesenchymal Cells
MMP14
MMP2
ANGPTL2
C1S
MFGE8
DFNA5
BMP1
C1R
MXRA8
MME
DDR2
ANTXR1
CYP1B1
LRP1
MAP1B
MTHFD1L
CTSF
NNT
LUM
COL6A6
CDH13
MECP2
ARHGEF17
ARHGAP42
COL6A5
NID1
DPYSL3
MACF1
CSPG4
COL5A1
MAMDC2
CALD1
CORO2B
EFEMP1
A2M
COL14A1
MAOB
COL3A1
DMD
AKAP12
DAAM2
MYL9
LDB3
NEXN
AOC3
MYLK
CNN1
ABCA8
ADARB1
MRVI1
MYH11
MYH10
ASPA
ADH1B
LSAMP
DES
CA3
CSRP1
LMOD1
CFD
ANO1
A B C D
2
0
-2
Immune Cells
ACP5
CTSB
NEU1
CAPG
CSTB
CTSS
BCAT1
ANPEP
CTSD
CYP27A1
MANBA
MAN2B1
APOE
MYO1G
CYBB
ATP6V1F
C5AR1
MAN2B2
ATP6V0D1
ACOT8
CCDC88A
CYBA
CD163
ARAP1
CPVL
LMNB1
ALOX5
BAZ1A
CD274
CD14
CORO1A
CRIP1
MNDA
A B C D
Endothelial Cells
AK4
ITGA2
ANGPT2
CPD
MOV10
ME3
ATP8B1
MYO6
NFAT5
NEDD4
ADAMTS4
ARGLU1
DDX60
MCF2L
CAV2
IFIT3
FGD5
CEP135
CAV1
BCAM
MYZAP
CRIP2
NES
IDO1
KCTD12
CD109
CRMP1
CDH5
CA4
NOSTRIN
COL15A1
MMRN2
A B C D
Epithelial Cells
DHCR24
LMO7
ALDH3A1
MACC1
ACAT2
DSG2
CLIC6
ARHGEF16
AGR3
LIMD1
AQP4
CAP2
CA2
CP
CLIC5
CTSH
CACNA2D2
CRYM
ALDH1A1
ALDH3B1
CD38
NEBL
AZGP1
AGER
APOH
A B C D
Commonly used lung cell-type markers
Cell-Type
Marker
Endothelial
PECAM1
VascularEndo
CD34
VascularEndo
CDH5
VascularEndo
VWF
LymphaticEndo
LYVE1
ciliated
TUBA4A
ATI
AGER
ATII
SFTPB
ATII
SFTPC
ATII
SFTPD
Epethelial
ABCA3
Epethelial
CDH1
Epethelial
EPCAM
fibroblast
TNC
fibroblast
PDGFRA
fibroblast
VIM
Pericytes
CSPG4
Pericytes
MCAM
Pericytes
NOTCH3
Pericytes
PDGFRB
Myofibroblast
EDNRB
Myofibroblast
MYH11
Myofibroblast
MYL9
Myofibroblast
MYLK
Myofibroblast
TAGLN
Myofibroblast
TGFBI
Macrophage
CD163
Macrophage
PTPRC
Dendritic cells
ITGAX
Myeloid cell
CTSS
A B C D

Figure S2

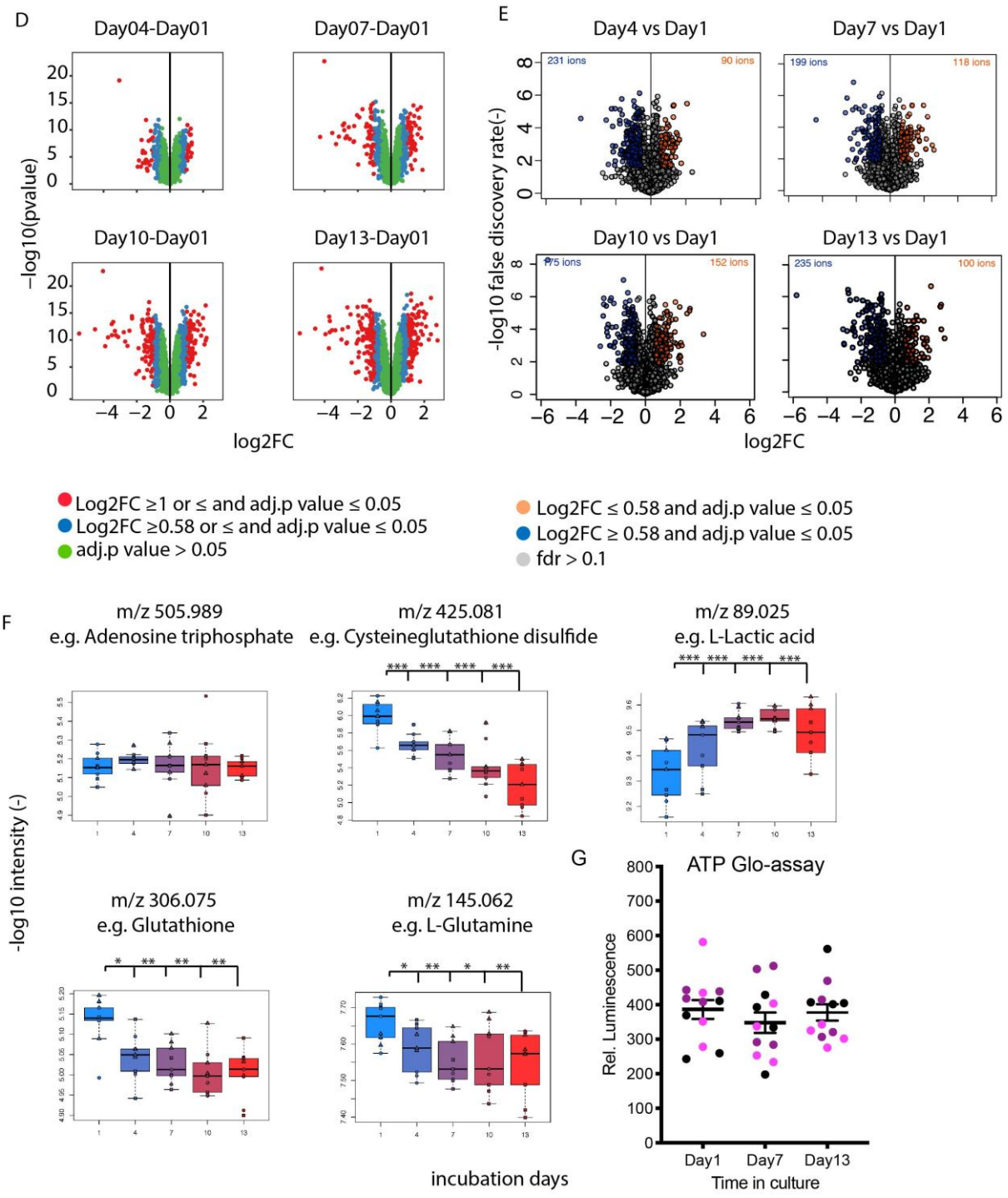
D
Day04-Day01
Day07-Day01
Day10-Day01
Day13-Day01
−log10(pvalue)
log2FC
E
Day4 vs Day1
Day7 vs Day1
Day10 vs Day1
Day13 vs Day1
231 ions
90 ions
199 ions
118 ions
175 ions
152 ions
235 ions
100 ions
-log10 false discovery rate(-)
log2FC
Log2FC ≥1 or ≤ and adj.p value ≤ 0.05
Log2FC ≥0.58 or ≤ and adj.p value ≤ 0.05
adj.p value > 0.05
Log2FC ≤ 0.58 and adj.p value ≤ 0.05
Log2FC ≥ 0.58 and adj.p value ≤ 0.05
fdr > 0.1
F
m/z 505.989
e.g. Adenosine triphosphate
m/z 425.081
e.g. Cysteineglutathione disulfide
m/z 89.025
e.g. L-Lactic acid
m/z 306.075
e.g. Glutathione
m/z 145.062
e.g. L-Glutamine
-log10 intensity (-)
incubation days
G
ATP Glo-assay
Rel. Luminescence
Day1
Day7
Day13
Time in culture

Figure S4

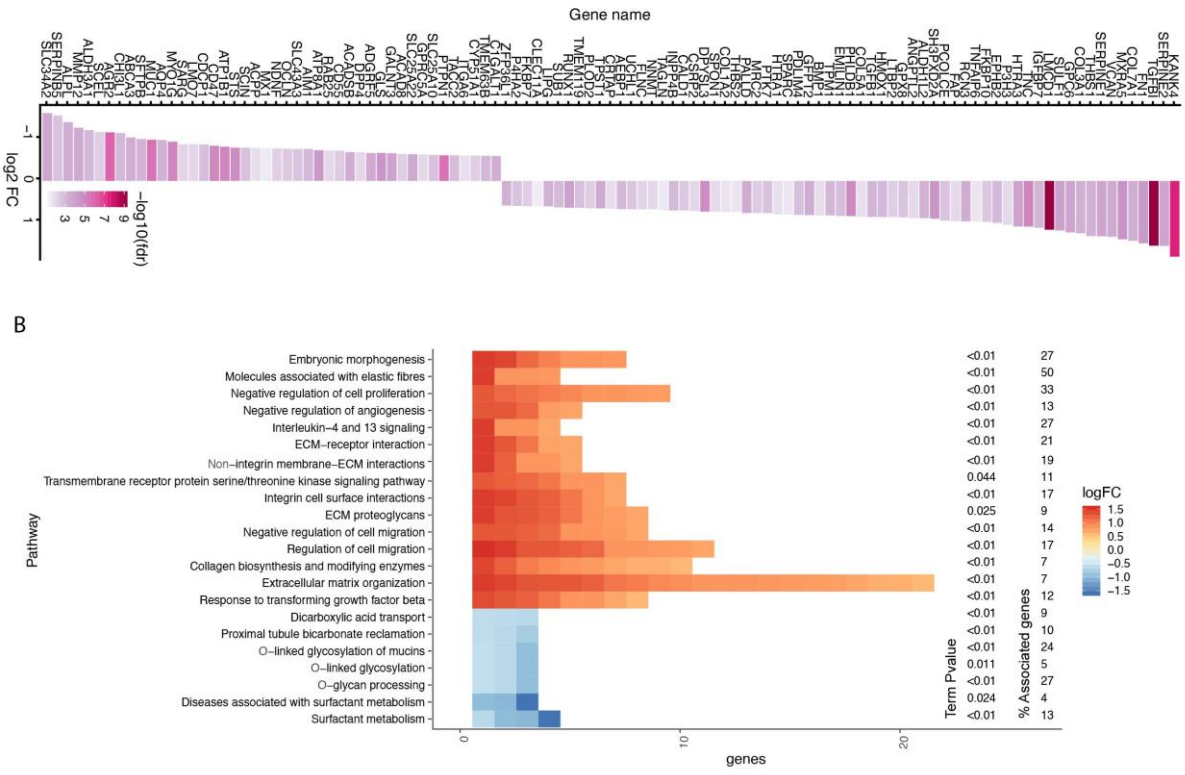

Significantly regulated proteome and related signalling pathways upon TGFbeta stimulation of ex vivo cultured hPCLS

Figure S4

C

Epethelial and Mesenchymal Cell class analysis of TGFß1 (vs Day13 vehicle treated) treated hPCLS proteome

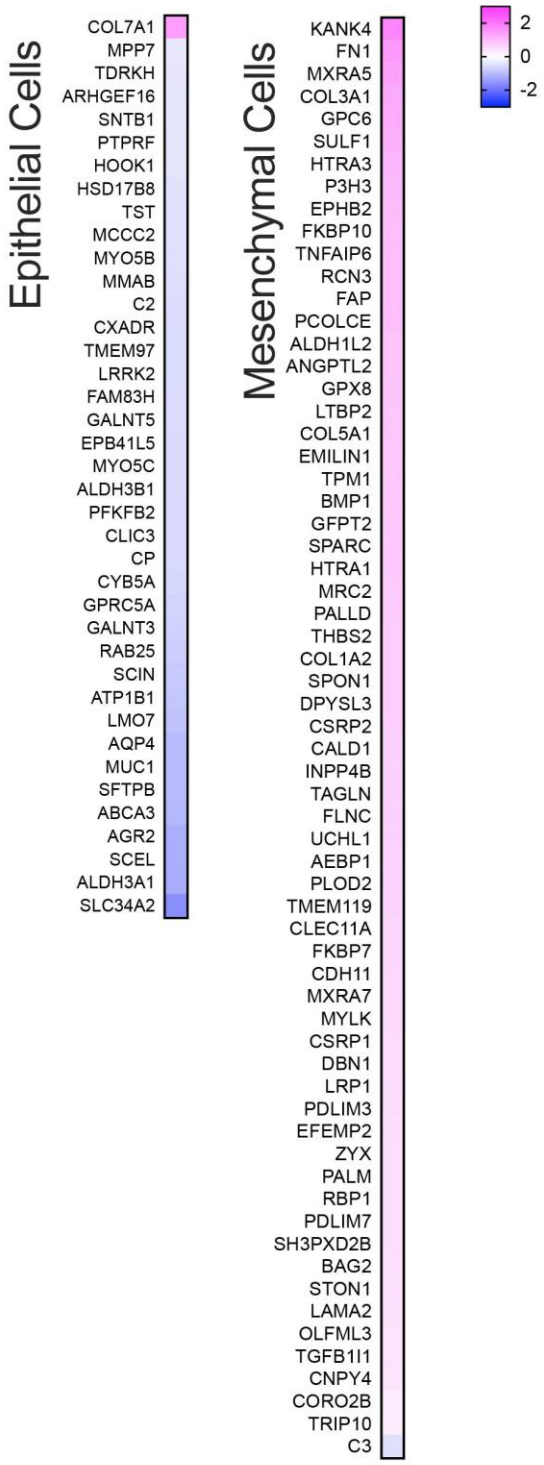

Figure S5

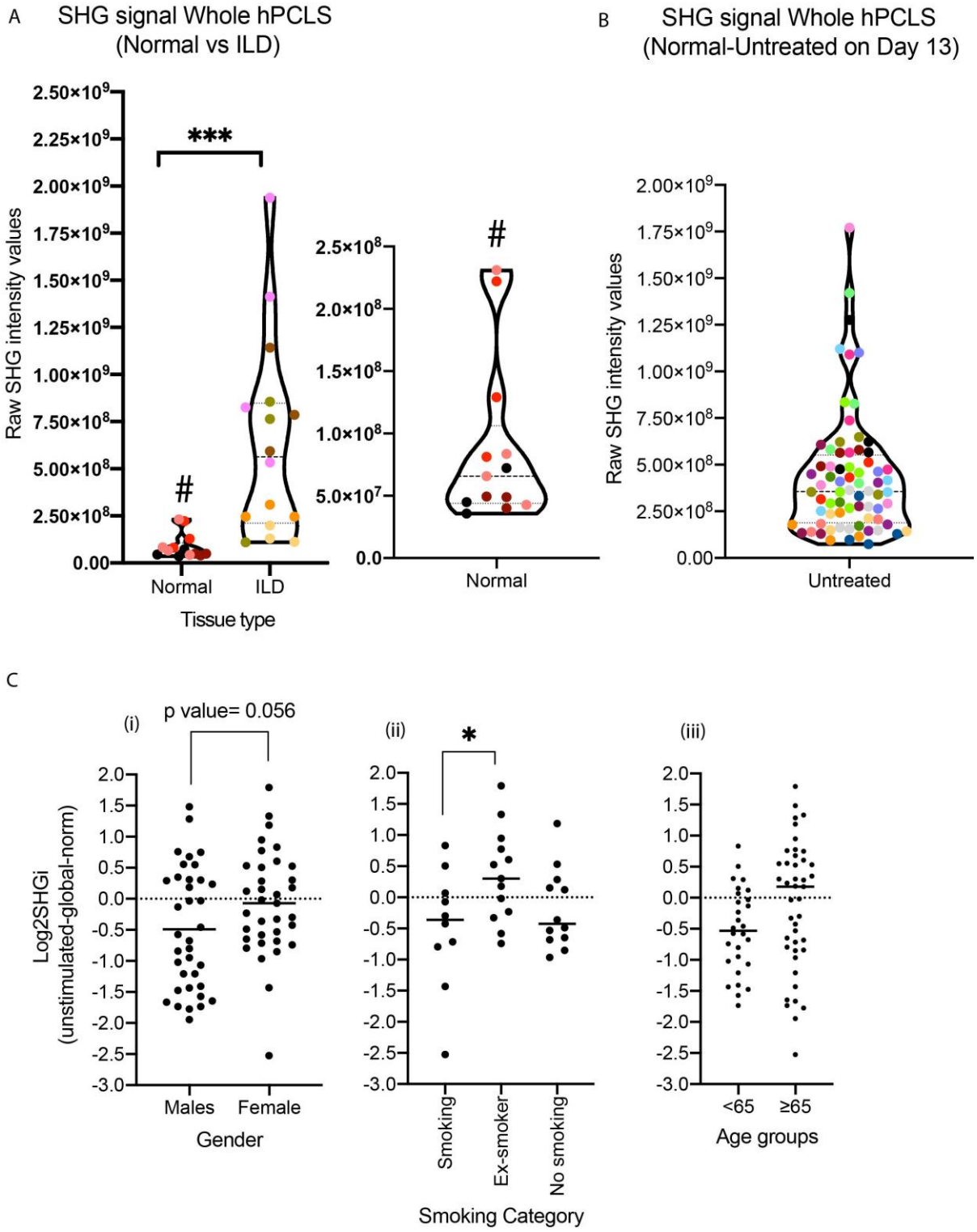
A
SHG signal Whole hPCLS
(Normal vs ILD)
Raw SHG intensity values
***
#
#
Normal
ILD
Tissue type
Normal
B
SHG signal Whole hPCLS
(Normal-Untreated on Day 13)
Raw SHG intensity values
Untreated
C
(i)
p value= 0.056
Log2SHGi
(unstimulated-global-norm)
Males
Female
Gender
(ii)
*
Smoking
Ex-smoker
No smoking
Smoking Category
(iii)
<65
≥65
Age groups

Figure S5D

Donor centric analysis of TGFß1 response:

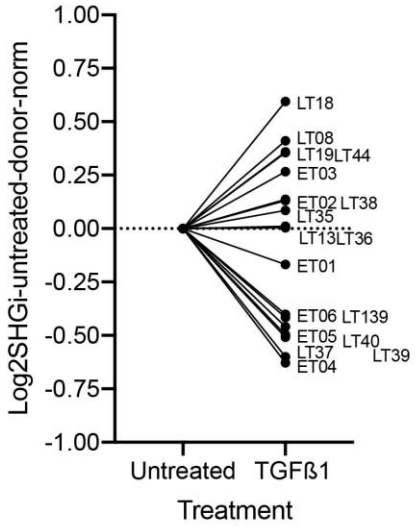

Gender centric analysis of TGFß1 response:

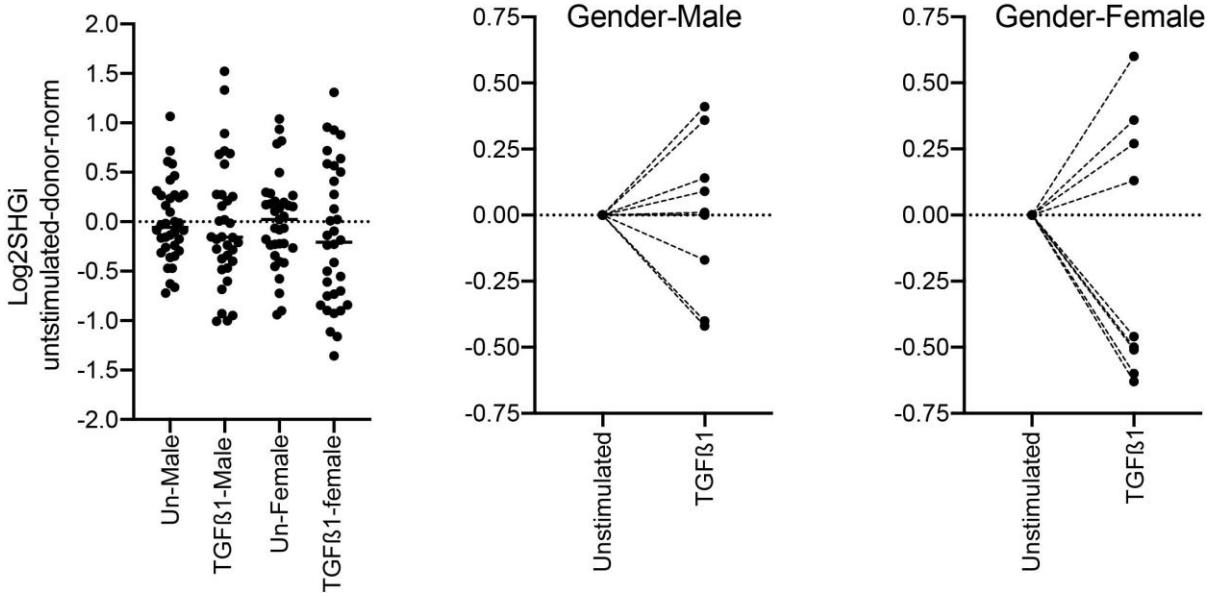

Figure S5E Smoking status centric analysis of TGFß1 response:

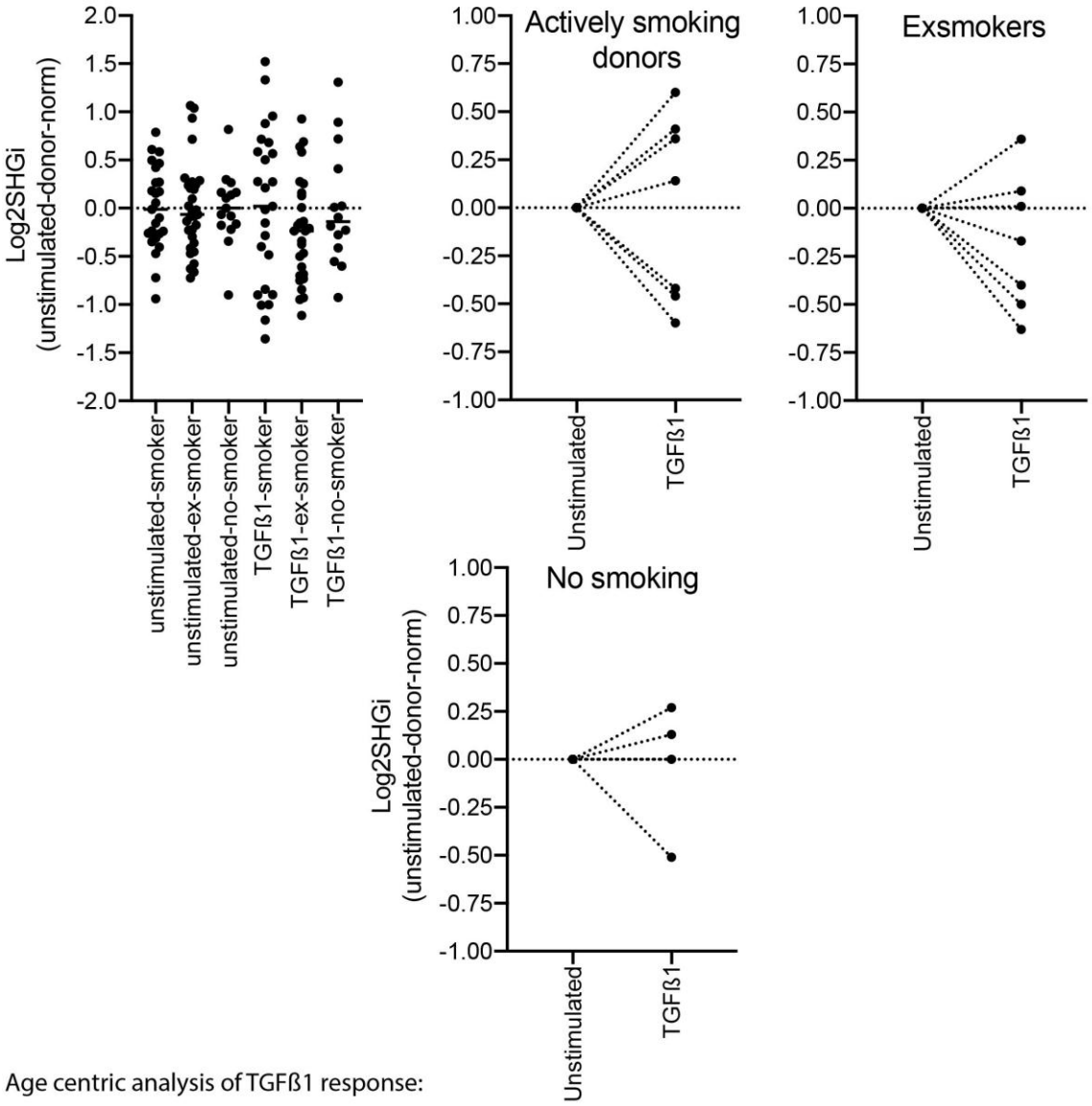

Age centric analysis of TGFß1 response:

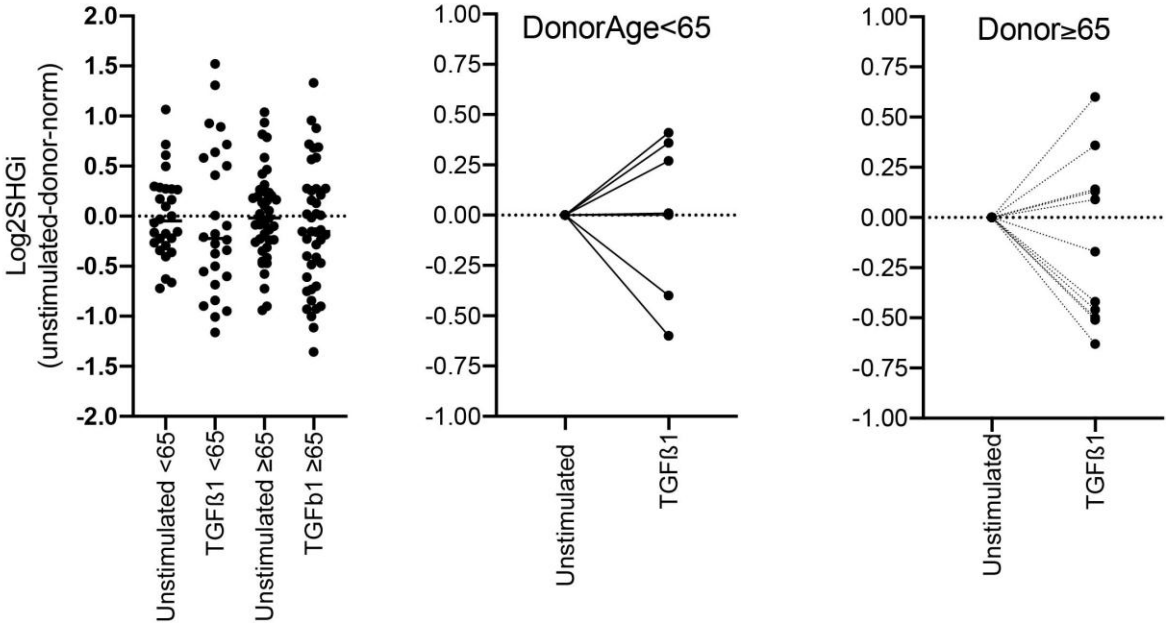

Figure S6: Live time lapse imaging